

UniADC: A Unified Framework for Anomaly Detection and Classification

Ximiao Zhang, Min Xu, Zheng Zhang, Junlin Hu, and Xiuzhuang Zhou

Abstract—In this paper, we introduce a novel task termed unified anomaly detection and classification, which aims to simultaneously detect anomalous regions in images and identify their specific categories. Existing methods typically treat anomaly detection and classification as separate tasks, thereby neglecting their inherent correlations and limiting information sharing, which results in suboptimal performance. To address this, we propose UniADC, a model designed to effectively perform both tasks with only a few or even no anomaly images. Specifically, UniADC consists of two key components: a training-free Controllable Inpainting Network and an Implicit-Normal Discriminator. The inpainting network can synthesize anomaly images of specific categories by repainting normal regions guided by anomaly priors, and can also repaint few-shot anomaly samples to augment the available anomaly data. The implicit-normal discriminator addresses the severe challenge of the imbalance between normal and anomalous pixel distributions by implicitly modeling the normal state, achieving precise anomaly detection and classification by aligning fine-grained image features with anomaly-category embeddings. We conduct extensive experiments on three anomaly detection and classification datasets, including MVTec-FS, MTD, and WFDD, and the results demonstrate that UniADC consistently outperforms existing methods in anomaly detection, localization, and classification. The code is available at <https://github.com/cnulab/UniADC>.

Index Terms—Anomaly detection, anomaly classification, anomaly synthesis, industrial defect inspection.

I. INTRODUCTION

IMAGE anomaly detection aims to train models to detect and localize anomalous regions within images. It has numerous practical applications and has attracted growing research interest in recent years [1]–[4]. Anomaly classification further categorizes detected anomalies, which aids in assessing anomaly severity and facilitating root-cause analysis. For instance, severe anomalies like scratches and breakage significantly compromise product quality, necessitating immediate production halts for inspection. Conversely, minor anomalies like stains or foreign matter have a negligible impact and are typically not classified as genuine defects. Existing studies [5], [6] typically treat anomaly classification as a downstream task of anomaly detection, in which the detected anomalous regions are cropped into sub-images and then fed

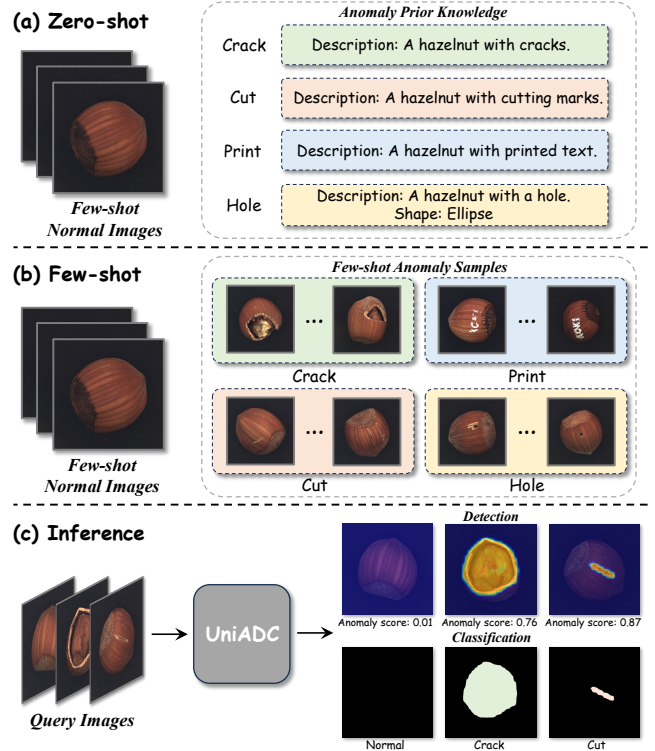


Fig. 1. Task settings for unified anomaly detection and classification. (a) Zero-shot: training with a few normal samples and prior knowledge for each anomaly category. (b) Few-shot: training with a few normal samples and few-shot anomaly samples per category. (c) Inference: UniADC predicts anomaly scores and categories for query images.

into a separate classification model. This two-stage pipeline ignores the inherent connection between anomaly detection and classification, and hinders information sharing across the two tasks. Moreover, missed and over detections during the detection stage, as well as the difficulty in selecting appropriate anomaly score thresholds, pose a series of challenges for subsequent classification. As a result, such methods often suffer from high implementation complexity and suboptimal performance, limiting their practicality in real-world scenarios.

In this paper, we integrate anomaly detection and classification tasks and address them with a unified model. We propose zero-shot and few-shot settings for unified anomaly detection and classification, both extending the widely studied few-shot anomaly detection task [7]–[10]. Few-shot anomaly detection provides only a small number of normal samples for model training, thereby reducing data collection costs, and has been widely applied in industrial [7]–[9] and medical [11], [12] fields. This setting is highly aligned with anomaly

This work was funded in part by the National Natural Science Foundation of China under Grants 62576049 and 61972046. (Corresponding author: Xiuzhuang Zhou.)

Ximiao Zhang, Zheng Zhang, and Xiuzhuang Zhou are with the School of Intelligent Engineering and Automation, Beijing University of Posts and Telecommunications, Beijing 100876, China. (E-mail: 2024010482@bupt.cn; zhangzheng@bupt.edu.cn; xiuzhuang.zhou@bupt.edu.cn).

Min Xu is with the College of Information and Engineering, Capital Normal University, Beijing 100048, China. (E-mail: xumin@cnu.edu.cn).

Junlin Hu is with the School of Software, Beihang University, Beijing 100191, China. (E-mail: hujunlin@buaa.edu.cn).

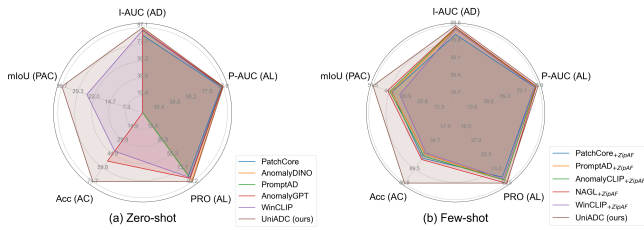


Fig. 2. Comparison of UniADC with alternative methods on the MVTEC-FS dataset. UniADC demonstrates superior performance over existing methods in Anomaly Detection (AD), Anomaly Localization (AL), Anomaly Classification (AC), and Pixel-level Anomaly Classification (PAC).

classification tasks in which available data is limited. Building upon this, the zero-shot anomaly detection and classification task does not provide additional anomaly samples for model training, but instead offers prior knowledge about anomaly categories, such as textual descriptions or shape information. This setting simulates real-world scenarios where collecting anomalous data is challenging. Differently, the few-shot anomaly detection and classification task provides a small number of anomaly samples for each category during model training, simulating practical scenarios where anomalous data is limited. Further explanation of the two settings is provided in Fig. 1.

To address the above tasks, we propose UniADC, a unified model for anomaly detection and classification, which tackles the challenge of scarce anomalous data through controllable image inpainting. It consists of two key components: a training-free controllable inpainting network and an implicit-normal discriminator. The controllable inpainting network consists of a pre-trained latent diffusion model [13] and an inpainting control network [14], enabling controllable inpainting guided by either anomaly priors or anomaly samples. Specifically, anomaly prior-guided controllable inpainting synthesizes category-specific anomalous images by repainting normal regions according to the provided prior knowledge of anomalies, whereas anomaly sample-guided controllable inpainting refines and repaints few-shot anomalous samples to enhance data diversity. In addition, we propose a category consistency selection strategy to filter synthetic anomaly samples that are highly consistent with the target category. The implicit-normal discriminator is trained on these synthetic anomaly samples and mitigates performance degradation caused by pixel-level distribution imbalance by disentangling the normal state from various anomaly concepts, thereby enabling robust anomaly detection and classification. Through the aforementioned innovative designs, UniADC comprehensively outperforms existing methods in anomaly detection, localization, and classification, as shown in Fig. 2, particularly strengthening the reliability of defect categorization. Our main contributions are summarized as follows:

- We introduce the task of unified anomaly detection and classification, which has broad application prospects yet remains underexplored. To this end, we propose UniADC, which enables accurate anomaly detection and classification under both zero-shot and few-shot settings.

- We propose a training-free controllable inpainting network that can generate category-specific anomaly samples conditioned on either anomaly prior or few-shot anomaly images. This enables broad applicability across various anomaly detection and classification tasks, serving as an effective alternative to existing anomaly synthesis methods.
- We propose an implicit-normal discriminator that mitigates performance degradation arising from the long-tail effect of anomaly data by implicitly modeling normal concepts, enabling it to effectively align fine-grained image features with anomaly-category embeddings for end-to-end anomaly detection and classification.
- Extensive experiments on the MVTEC-FS [5], MTD [15], and WFDD [16] demonstrate the effectiveness of UniADC and highlight its potential for real-world anomaly detection and classification applications.

II. RELATED WORK

A. Anomaly Detection

Image anomaly detection has gained widespread attention in recent years, leading to extensive research. Due to the scarcity of anomaly samples in real-world scenarios, most methods [17]–[21] follow an unsupervised paradigm, training solely on normal data and identifying anomalies that deviate from normal patterns during inference. However, in practical production scenarios, anomaly information is not entirely out of reach. Consequently, recent studies have explored integrating anomaly priors or limited anomaly samples into the detection pipeline to improve reliability. For example, PromptAD [8] employs textual descriptions of each anomaly category to improve detection accuracy. AnomalyGPT [9] predefines the expected appearance of query images and potential anomaly types to enhance the reasoning capability of the anomaly question answering model. AnoGen [22] integrates size priors of different anomaly types into the anomaly synthesis pipeline to ensure class consistency of the synthesized anomaly samples. BGAD [23] and NAGL [24] leverage a small number of anomaly samples to refine the model’s decision boundary, thereby bolstering its discriminative capability for more accurate detection. Motivated by these advances and real-world requirements, we systematically integrate diverse anomaly priors and limited anomaly samples into a unified anomaly detection and classification pipeline, and propose UniADC, a general framework that functionally extends existing methods.

B. Anomaly Classification

Anomaly classification aims to identify the categories of detected anomalous regions, which remains highly challenging due to the scarcity of anomaly samples. Despite its broad range of applications, this field has not yet been extensively explored. ZipAF [5] employs the AlphaCLIP model [25] to extract region-contextual anomaly features and adopts a zero-initialized projection to align query features with cached anomaly features for few-shot anomaly classification. However, it does not incorporate the anomaly detection process,

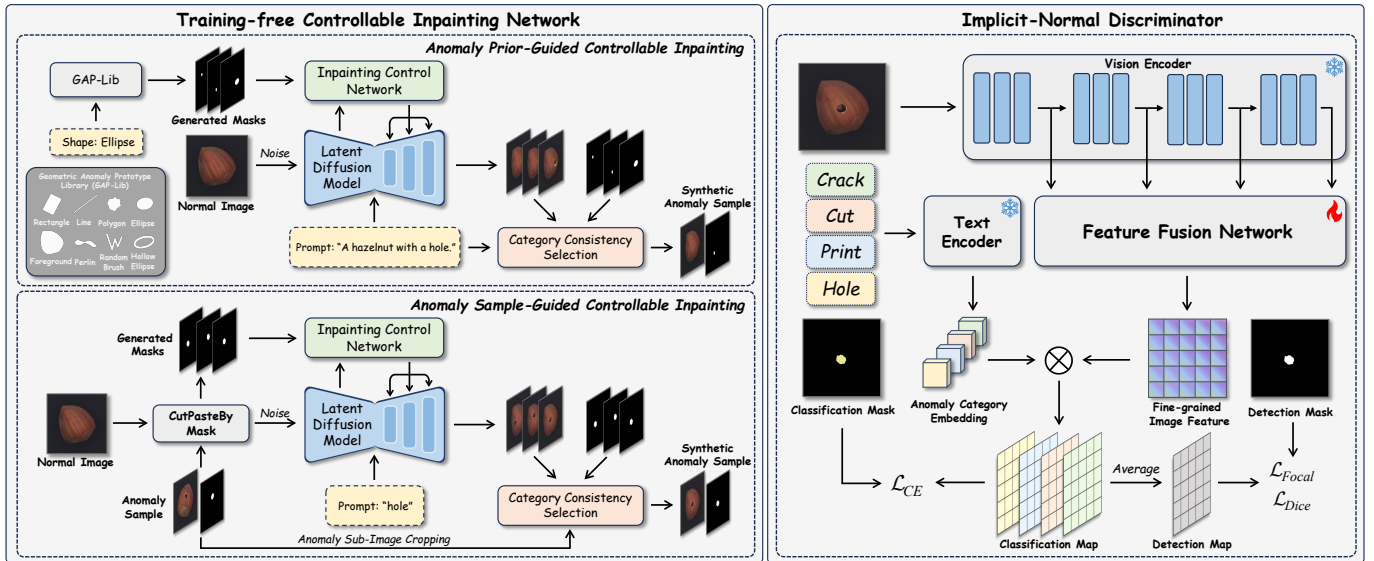


Fig. 3. Overview of the proposed UniADC pipeline, which consists of a training-free controllable inpainting network and an implicit-normal discriminator. The controllable inpainting network supports two modes: anomaly prior-guided controllable inpainting and anomaly sample-guided controllable inpainting, enabling the generation of category-specific anomaly samples under different settings. The implicit-normal discriminator aligns fine-grained image features with anomaly category embeddings for accurate anomaly detection and classification.

which may result in degraded performance in practical scenarios. AnomalyNCD [6] integrates novel class discovery methods into the existing anomaly detection pipeline for anomaly detection and clustering. Recent work [26] proposes a zero-shot multi-type anomaly detection method, MultiADS, which trains the model to learn cross-domain anomaly priors for anomaly classification. However, due to the lack of targeted training, this method struggles to identify domain-specific anomaly types, such as identifying highly similar defects within a specific product [15], [27], [28].

C. Anomaly Synthesis

Existing anomaly synthesis methods can generally be classified into zero-shot and few-shot approaches, depending on the availability of real anomaly data during the synthesis process [29]. Zero-shot approaches generate anomaly samples relying on predefined data augmentation rules [30]–[32], noise injection [33], [34], or textual descriptions [35], [36], without access to real anomaly samples. However, the synthesized anomalies may exhibit a distribution shift from real-world cases, limiting their effectiveness. In contrast, few-shot approaches [37]–[40] aim to enhance data diversity by augmenting a limited number of real anomaly samples. Despite significant progress in anomaly synthesis techniques, existing research remains primarily focused on anomaly detection. The category controllability and accuracy of synthesized anomaly samples still require further validation to ensure their feasibility for more challenging anomaly classification tasks.

III. METHOD

In this section, we present our proposed anomaly detection and classification model, UniADC, with its overall pipeline illustrated in Fig. 3. We first provide the problem definition, then

describe the main functionalities and implementation details of the controllable inpainting network, including anomaly prior-guided controllable inpainting and anomaly sample-guided controllable inpainting. Finally, we introduce the implicit-normal discriminator of UniADC.

A. Problem Definition

In few-shot anomaly detection, the model is provided with a support set of normal samples $\mathcal{D}^n = \{X_1, X_2, \dots, X_{K_n}\}$, where K_n denotes the number of normal samples per image class. Given a query image, the model predicts an image-level anomaly detection score $I_d \in [0, 1]$ and a pixel-level anomaly map $S_d \in [0, 1]^{H \times W}$, where H and W denote the image height and width, respectively. The zero-shot and few-shot anomaly detection and classification tasks respectively provide additional anomaly prior knowledge and an anomaly support set for model training. Specifically, the anomaly support set is represented as $\mathcal{D}^a = \bigcup_{y \in \{1, 2, \dots, Y\}} \{(X_1^y, M_1^y), (X_2^y, M_2^y), \dots, (X_{K_a}^y, M_{K_a}^y)\}$, where Y denotes the number of anomaly categories, K_a is the number of samples per anomaly category, and M denotes the binary anomaly mask. The model is further trained to predict both an image-level classification result $I_c \in \{0, 1, \dots, Y\}$ and a pixel-level classification result $S_c \in \{0, 1, \dots, Y\}^{H \times W}$, where 0 indicates the normal class, and 1 to Y represent the Y anomaly categories.

B. Anomaly Prior-Guided Controllable Inpainting

This module synthesizes category-specific anomaly samples based on provided anomaly priors, making it suitable for zero-shot anomaly detection and classification tasks. The anomaly prior includes the shape, size, and textual description of each anomaly category. Shape and size are used to generate the

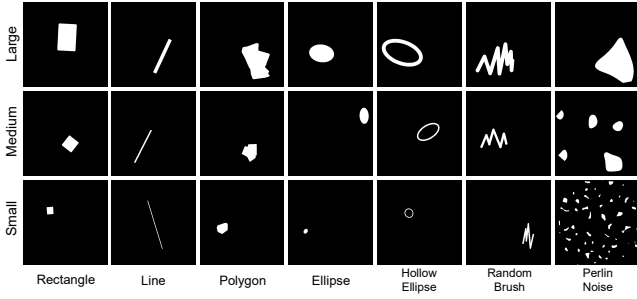


Fig. 4. Examples of anomaly masks generated from the GAP-Lib.

anomaly mask, while the textual description serves as a prompt to guide the synthesis of the desired anomalous appearance. Specifically, to map various anomaly shapes and sizes into explicit spatial constraints, we constructed a Geometric Anomaly Prototype Library (GAP-Lib). It comprises eight types of candidate masks, including *Rectangle*, *Line*, *Polygon*, *Ellipse*, *Hollow Ellipse*, *Random Brush*, *Perlin Noise*, and *Foreground Mask*. The first seven types are used to simulate various local anomalous regions, with each type defined in three sizes: *Large*, *Medium*, and *Small*, as illustrated in Fig. 4. Each mask size corresponds to a specific size range. *Foreground Mask* uses the object’s foreground as a mask to synthesize global anomalies. We use specific mask types for mask generation based on the given anomaly shape and size. For example, we specify the shape of the anomaly category “Hole” as *Ellipse*, which will generate elliptical masks of arbitrary sizes. When both shape and size priors are unavailable for an anomaly category, all mask types are used for mask generation.

For a given normal image X and prior knowledge from anomaly category y , we first generate an anomaly mask M^y utilizing the proposed GAP-Lib. Then, the latent diffusion model encodes the image X and the text prompt p^y into latent variables $z = \mathbb{E}_v(X)$ and $z^p = \mathbb{E}_t(p^y)$, where $\mathbb{E}_v(\cdot)$ and $\mathbb{E}_t(\cdot)$ denote the vision and text encoders, respectively. We define the number of forward diffusion steps as $T' = T \cdot \gamma$, where T denotes the total number of diffusion steps in the original latent diffusion model, and $\gamma \in (0, 1]$ controls the noise strength. A larger γ injects more noise into the latent variable, resulting in synthesized anomalies that deviate further from the original image distribution and exhibit more visually prominent anomalous patterns. To ensure spatial consistency between synthesized anomalies and the anomaly mask, we use an inpainting control network to precisely control the locations of the synthesized anomalies. Specifically, at each time step $t \in \{1, 2, \dots, T'\}$, the inpainting control network ϕ predicts the conditioning variable $z^m = \phi(z_t, t, z, M^y)$ of noisy latent z_t for controlling the denoising process:

$$z_{t-1} = \Psi(z_t, t, z^p, z^m) \quad (1)$$

where Ψ denotes the latent diffusion model, and the conditioning variables z^p and z^m respectively control the semantics and spatial positions of the synthesized anomalies. The inpainting control network ensures that the denoised latent representation z_0 remains consistent with the original latent z outside the masked region, while repainting only the masked region to

align with the prompt embedding z^p . Finally, the denoised latent representation z_0 is decoded by decoder $\mathbb{D}(\cdot)$ into the anomaly image $X^y = \mathbb{D}(z_0)$. In our implementation, we adopt Stable Diffusion v1.5 [13] as the latent diffusion model and integrate BrushNet [41] as a plug-and-play control network for inpainting. This configuration enables UniADC to achieve highly accurate control over anomaly placement and image-mask consistency, bypassing the need for costly post-processing or mask refinement steps common in other anomaly synthesis methods [35], [36], [39].

However, the above synthesis process does not ensure the semantic alignment between anomaly masks and their corresponding textual descriptions, which may lead to inconsistencies between the synthesized anomaly samples and their intended categories. For example, in the case of “*a broken transistor lead*”, the synthesized anomaly should be located in the lead region, rather than randomly elsewhere. To this end, we propose a Category Consistency Selection (CCS) strategy to further filter synthetic anomalous images with high category consistency, thereby eliminating noisy samples introduced by anomaly synthesis. Given an anomaly category y , we first generate a mini-batch of synthesized samples using diverse anomaly masks, denoted as $\mathcal{S}^y = \{(X_b^y, M_b^y)\}_{b=1}^B$, where B is the mini-batch size. We then adopt the AlphaCLIP model [25] to evaluate the semantic consistency between the synthesized image-mask pairs and the textual description of the anomaly category. For the synthetic anomaly sample (X_b^y, M_b^y) , we calculate its category matching score as:

$$\mathcal{P}_b = \frac{\exp(\langle \psi_v(X_b^y, M_b^y), \psi_t(p^y) \rangle)}{\sum_{y \in \{1, 2, \dots, Y\}} \exp(\langle \psi_v(X_b^y, M_b^y), \psi_t(p^y) \rangle)} \quad (2)$$

where ψ_v and ψ_t denote the vision and text encoders of AlphaCLIP, respectively, and $\langle \cdot, \cdot \rangle$ denotes the inner product. The AlphaCLIP model aligns the image region features guided by the masks with the text embeddings. If the synthetic anomalous region fails to match the corresponding anomaly description, such as being placed in the wrong location, the matching score decreases. In the end, we select the synthetic anomaly sample with the highest matching score in the mini-batch \mathcal{S}^y for subsequent discriminator training.

C. Anomaly Sample-Guided Controllable Inpainting

Anomaly sample-guided controllable inpainting aims to enrich the diversity of anomalies by repainting few-shot anomaly samples, making it well-suited for few-shot anomaly detection and classification tasks. Given a normal image X and an anomalous sample (X^y, M^y) , we first crop the anomalous region from X^y based on the mask M^y , and paste it at a random location on the normal image X , yielding a preliminary synthetic anomaly image \hat{X}^y and its corresponding mask \hat{M}^y . To increase the shape variation, we apply identical data augmentations, such as affine transformations, to both the anomalous region and its mask. However, at this stage, the synthesized anomalies still suffer from limited diversity and suboptimal visual coherence. To improve diversity and image quality, we use the latent diffusion model along with an inpainting control network to repaint the pasted regions in

TABLE I
COMPARISON BETWEEN UNIADC AND ALTERNATIVE ANOMALY SYNTHESIS METHODS. NOTE: “TRAINING-FREE” SPECIFICALLY CHARACTERIZES THE ANOMALY SYNTHESIS STAGE, INDEPENDENT OF THE SUBSEQUENT TRAINING OF THE DETECTION MODEL.

Method	Training-free	Zero-shot Generation	Few-shot Generation	Diversity Mask	Controllable Anomaly Types
DR/EM [43]	✓	✓	✗	✗	✗
RealNet [34]	✗	✓	✗	✗	✗
AnoGen [22]	✗	✗	✓	✗	✓
AnomalyDiff [38]	✗	✗	✓	✓	✓
DualAnoDiff [39]	✗	✗	✓	✓	✓
AnomalyAny [35]	✓	✓	✗	✓	✓
UniADC (ours)	✓	✓	✓	✓	✓

\hat{X}^y . The repainting process is guided by simple text prompts (e.g., the name of the anomaly category) and follows the same diffusion and denoising procedures as described in anomaly prior-guided inpainting. The degree of diversity and deviation from the original anomaly is controlled by the noise factor γ . To ensure semantic consistency, we perform category consistency selection by computing the Structural Similarity Index (SSIM) [42] between the original and repainted anomalous sub-images. These sub-images include both the anomalous region and a fixed amount of surrounding normal context. We compute the SSIM-based category matching score for each sample and retain the highest-scoring synthetic anomaly sample for discriminator training. Table I compares UniADC with other anomaly synthesis methods. To the best of our knowledge, UniADC is the first method capable of synthesizing anomalies under both zero-shot and few-shot settings. Moreover, it supports both diverse mask generation and fine-grained control over anomaly categories, thereby significantly enhancing its applicability across a wide range of anomaly detection and classification tasks.

D. Implicit-Normal Discriminator

Beyond the challenge of scarce anomalous samples, another core difficulty in anomaly detection and classification lies in the severe distribution imbalance between normal pixels and various categories of anomalous pixels. Conventional discriminative anomaly detection models [8], [26], [44] typically align image patch features with class embeddings corresponding to “normal” and “anomaly” concepts through adapter fine-tuning or learnable text prompts. However, for multi-class anomaly classification, the long-tail effect of the data is significantly exacerbated. This causes such methods to inevitably overfit to the massive volume of normal pixels, ultimately leading to performance degradation in both anomaly detection and classification. To mitigate this, we propose the Implicit-Normal Discriminator (IND). Our key insight is to eliminate the explicit category embedding for the normal state. Instead of treating “normal” as a distinct class, we identify normal regions by the absence of all potential anomaly types. This exclusion-based logic forces the model to focus exclusively on the manifold of diverse anomaly concepts, thereby substantially alleviating the bias induced by imbalanced data distributions. Specifically, the proposed implicit-normal discriminator

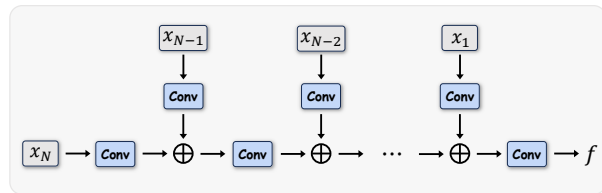


Fig. 5. Architecture of the Feature Fusion Network.

is trained using synthetic anomalous samples to align fine-grained image features with anomaly category embeddings, thereby enabling unified anomaly detection and classification. First, we represent each synthetic anomalous sample as a 4-tuple (X, y, M_d, M_c) , where X is the synthesized anomalous image, y is the anomaly category label, and M_d and M_c respectively denote the anomaly detection mask and classification mask, for a pixel location (i, j) satisfying:

$$M_c(i, j) = \begin{cases} y, & M_d(i, j) = 1 \\ 0, & M_d(i, j) = 0 \end{cases} \quad (3)$$

We employ a pre-trained vision encoder to extract multi-scale image features $\{x_1, x_2, \dots, x_N\} = \varphi(X)$, and fuse these features into a fine-grained representation through a Feature Fusion Network (FFN) $f = \theta(x_1, x_2, \dots, x_N)$, where $f \in \mathbb{R}^{H' \times W' \times C}$. As illustrated in Fig. 5, the FFN progressively aggregates intermediate-layer features from high to low semantic levels via a fully convolutional architecture. Concurrently, a text encoder embeds anomaly category names into a semantic space to obtain embeddings $\{g_1, g_2, \dots, g_Y\}$, where $g_y \in \mathbb{R}^C$. The similarity between the anomaly category embedding g_y and the feature map f at a spatial location (h, w) is computed as:

$$s_y(h, w) = \sigma(\langle f(h, w), g_y \rangle / \epsilon) \quad (4)$$

where $\sigma(\cdot)$ denotes the Sigmoid function, and ϵ is a learnable scaling parameter. We compute the similarity score at each spatial location and upsample the resulting similarity matrix to the original image resolution, yielding a classification map $S_y \in (0, 1)^{H \times W}$, which indicates the likelihood of anomaly category y at each pixel. By computing classification maps for all categories, we obtain a set of classification maps $\{S_1, S_2, \dots, S_Y\}$. The pixel-level anomaly detection map S_d is then computed as the average of these classification maps: $S_d = \frac{1}{Y} \sum_{y=1}^Y S_y$. The maximum value of S_d is used as the image-level anomaly detection score I_d . Then, the pixel-level anomaly classification result at a pixel location (i, j) is:

$$S_c(i, j) = \begin{cases} \operatorname{argmax}_{y \in \{1, 2, \dots, Y\}} S_y(i, j), & S_d(i, j) \geq \tau \\ 0, & S_d(i, j) < \tau \end{cases} \quad (5)$$

where τ represents the anomaly score threshold used to distinguish between normal and anomalous states. We use the anomaly category with the largest pixel area in S_c as the image-level anomaly classification result I_c . If all pixels in S_c are classified as normal, then I_c is set to 0. We optimize the feature fusion network using Binary Focal loss [45] and

TABLE II
COMPARISON OF UNIADC WITH ALTERNATIVE METHODS UNDER ZERO-SHOT ANOMALY DETECTION AND CLASSIFICATION SETTINGS. † DENOTES METHODS THAT USE ANOMALY PRIORS.

K_n	Method	MVTec-FS [5]					MTD [15]					WFDD [16]				
		I-AUC	P-AUC	PRO	Acc	mIoU	I-AUC	P-AUC	PRO	Acc	mIoU	I-AUC	P-AUC	PRO	Acc	mIoU
1	InCTRL [47]	92.36	-	-	-	-	70.34	-	-	-	-	96.66	-	-	-	-
	PatchCore [17]	84.76	93.77	82.44	-	-	68.22	73.44	59.50	-	-	84.81	96.07	70.62	-	-
	AnomalyDINO [48]	96.12	96.54	89.04	-	-	85.32	78.01	74.11	-	-	97.42	98.86	87.88	-	-
	† PromptAD [8]	91.80	95.09	87.06	-	-	86.27	71.70	70.61	-	-	96.90	97.10	86.72	-	-
	† AnomalyGPT [9]	93.48	95.92	86.60	45.85	-	71.91	68.41	58.67	27.57	-	96.89	97.72	85.69	45.76	-
	† WinCLIP [7]	93.20	94.43	86.47	40.75	25.17	77.53	69.26	57.58	28.69	15.10	95.72	93.94	78.98	34.64	27.53
	† UniADC (CLIP)	95.03	96.33	88.75	66.07	32.90	86.19	80.80	77.69	55.82	27.92	97.01	99.00	87.03	86.70	45.55
† UniADC (DINO)	96.37	96.11	89.16	68.30	35.06	90.09	82.65	79.98	59.22	29.58	98.08	99.46	92.13	88.88	52.17	
2	InCTRL [47]	93.01	-	-	-	-	72.07	-	-	-	-	97.36	-	-	-	-
	PatchCore [17]	88.49	94.43	84.65	-	-	69.90	75.07	60.52	-	-	88.06	96.35	71.45	-	-
	AnomalyDINO [48]	96.87	97.14	90.96	-	-	86.32	79.27	76.82	-	-	97.72	99.13	89.03	-	-
	† PromptAD [8]	93.95	95.42	87.93	-	-	87.06	73.53	69.91	-	-	97.15	97.20	86.81	-	-
	† AnomalyGPT [9]	94.91	96.24	87.97	52.65	-	72.57	70.20	60.12	32.56	-	97.48	97.78	85.75	47.39	-
	† WinCLIP [7]	94.37	94.60	86.95	41.93	25.34	78.07	71.57	57.70	29.90	15.28	96.50	94.16	80.19	35.83	27.62
	† UniADC (CLIP)	95.27	96.53	88.52	71.64	35.12	90.31	82.92	78.99	62.87	30.56	97.55	98.98	87.14	89.48	48.15
† UniADC (DINO)	97.09	97.04	92.15	74.74	36.66	92.30	83.52	81.22	64.15	31.85	98.21	99.46	92.35	89.22	53.38	
4	InCTRL [47]	93.62	-	-	-	-	73.23	-	-	-	-	97.38	-	-	-	-
	PatchCore [17]	90.75	95.28	86.56	-	-	71.40	75.35	59.67	-	-	88.26	97.21	71.41	-	-
	AnomalyDINO [48]	97.50	97.30	92.21	-	-	89.68	83.11	78.61	-	-	98.15	99.43	91.54	-	-
	† PromptAD [8]	94.91	95.92	89.86	-	-	88.16	73.82	71.49	-	-	96.79	97.53	87.80	-	-
	† AnomalyGPT [9]	96.10	96.42	91.09	56.59	-	74.38	68.68	59.92	42.48	-	98.00	97.92	86.35	48.24	-
	† WinCLIP [7]	95.17	94.98	87.67	42.69	25.70	78.90	69.84	58.11	29.91	16.17	96.74	94.58	80.28	34.99	27.79
	† UniADC (CLIP)	96.18	96.47	91.17	73.33	35.14	90.88	84.88	79.81	63.98	31.29	98.15	99.09	88.29	90.85	48.24
† UniADC (DINO)	97.65	97.36	92.68	76.35	37.23	93.04	85.82	81.43	66.03	33.75	98.60	99.39	94.76	91.06	55.44	

Dice loss [46] for anomaly detection, and Cross-Entropy loss for anomaly classification. The overall loss function is:

$$\mathcal{L} = \mathcal{L}_{Focal}(S_d, M_d) + \mathcal{L}_{Dice}(S_d, M_d) + \lambda \mathcal{L}_{CE}([S_1, S_2, \dots, S_Y], M_c) \quad (6)$$

where $[\cdot, \cdot]$ denotes the concatenation operation, and λ is a weight hyperparameter. The normal regions in M_c are ignored during the computation of \mathcal{L}_{CE} . By excluding the normal category, our model is forced to refine the boundaries between various anomaly concepts, thereby enhancing its anomaly recognition performance and classification reliability.

IV. EXPERIMENT

To validate the effectiveness of our proposed UniADC framework, we conducted a comprehensive evaluation of its anomaly detection and classification performance on the MVTec-FS [5], MTD [15], and WFDD [16] datasets. This section provides a detailed account of the experimental setup, main experimental results and analysis, as well as a systematic ablation study.

A. Experimental Setup

1) *Datasets*. We conduct extensive evaluations on three anomaly detection and classification datasets, including MVTec-FS [5], MTD [15], and WFDD [16]. The MVTec-FS dataset is introduced by ZipAF [5] as an extension of the MVTec-AD benchmark [49] for anomaly classification. It contains 15 types of industrial products, each with an average of four anomaly categories. The MTD dataset [15] consists of 1,344 images of magnetic tiles, including five types of anomalies. The subtle differences among these anomalies make the classification task particularly challenging. The WFDD dataset

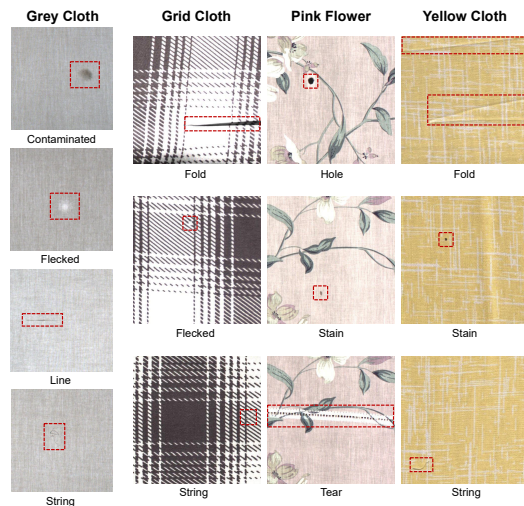


Fig. 6. Examples of different anomaly categories in the WFDD dataset, with anomalous regions marked by red bounding boxes.

[16] comprises 4,101 images across four fabric types: Grey Cloth, Grid Cloth, Pink Flower, and Yellow Cloth. Since it was originally designed for anomaly detection, it lacked a detailed categorization of anomaly types. To facilitate our proposed anomaly detection and classification task, we reclassified the dataset by grouping identical defects, resulting in an average of three anomaly categories per fabric. Representative examples for each category are illustrated in Fig. 6. Other widely-used anomaly detection datasets, such as VisA [50], are excluded from this work due to the lack of anomaly category labels.

2) *Implementation Details*. We adopt a consistent experimental setup for both anomaly prior-guided and anomaly sample-guided inpainting. Specifically, we use the DDIM sam-

TABLE III
COMPARISON OF UNIADC WITH ALTERNATIVE METHODS UNDER FEW-SHOT ANOMALY DETECTION AND CLASSIFICATION SETTINGS.

K_n	K_a	Method	MVTec-FS [5]					MTD [15]					WFDD [16]				
			I-AUC	P-AUC	PRO	Acc	mIoU	I-AUC	P-AUC	PRO	Acc	mIoU	I-AUC	P-AUC	PRO	Acc	mIoU
1	1	PatchCore+ZipAF [17]	84.76	93.77	82.44	52.10	37.30	68.22	73.44	59.50	28.26	20.33	84.81	96.07	70.62	61.75	39.10
		WinCLIP+ZipAF [7]	93.20	94.43	86.47	49.60	34.39	77.53	69.26	57.58	33.78	24.23	95.72	93.94	78.98	59.59	37.30
		PromptAD+ZipAF [8]	92.74	95.72	88.06	49.12	39.57	86.85	72.30	70.87	31.79	28.92	97.47	97.51	86.23	64.11	44.60
		AnomalyCLIP+ZipAF [44]	95.59	96.00	87.98	52.60	40.25	76.18	75.98	69.54	25.61	21.78	93.76	98.59	87.58	76.48	45.99
		NAGL+ZipAF [24]	95.60	96.51	92.79	55.92	42.00	84.98	75.45	75.77	36.37	30.89	97.20	98.93	92.40	71.82	45.32
		UniADC (CLIP)	97.69	98.53	89.72	84.72	48.62	88.49	82.41	77.41	60.81	34.80	98.50	98.83	92.96	93.51	48.76
		UniADC (DINO)	98.42	98.96	92.26	86.74	51.28	91.41	82.88	80.07	62.47	32.21	99.85	99.37	94.07	96.10	50.53
2	1	PatchCore+ZipAF [17]	88.49	94.43	84.65	56.16	39.63	69.90	75.07	60.52	30.15	21.03	88.06	96.35	71.45	63.82	39.71
		WinCLIP+ZipAF [7]	94.37	94.60	86.95	49.99	34.77	78.07	71.57	57.70	33.31	24.54	96.50	94.16	80.19	60.21	37.28
		PromptAD+ZipAF [8]	94.58	95.66	88.93	51.40	40.09	87.41	74.10	71.12	36.09	29.78	97.52	97.74	87.01	67.17	44.51
		AnomalyCLIP+ZipAF [44]	95.94	96.12	88.77	53.80	40.90	76.42	76.11	70.62	26.57	21.17	94.96	98.75	87.80	77.99	46.49
		NAGL+ZipAF [24]	96.41	96.56	92.96	57.78	42.34	84.92	77.71	77.72	39.75	31.49	97.47	98.89	92.60	72.40	47.19
		UniADC (CLIP)	98.35	98.63	90.64	85.20	48.93	90.70	84.49	80.71	63.78	35.58	98.97	99.16	94.64	93.66	49.71
		UniADC (DINO)	98.56	98.90	92.48	86.85	51.49	92.57	86.79	83.17	65.10	34.33	99.87	99.48	94.12	97.22	51.78
2	2	PatchCore+ZipAF [17]	88.49	94.43	84.65	58.25	40.32	69.90	75.07	60.52	34.71	21.78	88.06	96.35	71.45	64.52	41.29
		WinCLIP+ZipAF [7]	94.37	94.60	86.95	51.76	35.25	78.07	71.57	57.70	37.36	27.14	96.50	94.16	80.19	61.64	37.69
		PromptAD+ZipAF [8]	95.16	95.60	89.03	52.66	40.93	88.46	74.53	71.91	43.89	31.16	97.75	98.20	86.81	67.91	45.25
		AnomalyCLIP+ZipAF [44]	95.93	96.47	89.12	52.93	42.49	76.72	76.32	73.90	35.57	24.81	95.25	98.73	90.38	81.17	47.74
		NAGL+ZipAF [24]	96.74	97.17	92.80	61.33	45.30	85.77	80.46	78.18	47.21	35.01	97.56	98.90	92.90	76.49	48.85
		UniADC (CLIP)	98.75	98.88	93.31	89.88	54.93	93.15	86.20	83.36	71.34	37.05	99.14	99.34	94.85	94.90	51.06
		UniADC (DINO)	99.05	99.10	93.55	88.72	54.21	93.85	89.31	85.78	70.87	35.46	99.93	99.49	94.19	97.76	51.91
4	1	PatchCore+ZipAF [17]	90.75	95.28	86.56	60.32	39.80	71.40	75.35	59.67	31.58	21.92	88.26	97.21	71.41	64.17	42.93
		WinCLIP+ZipAF [7]	95.17	94.98	87.67	53.75	35.98	78.90	69.84	58.11	33.89	28.32	96.74	94.58	80.28	63.59	37.59
		PromptAD+ZipAF [8]	96.49	96.10	90.02	55.21	41.66	87.78	73.82	71.49	38.36	30.13	97.57	97.83	87.80	70.59	44.87
		AnomalyCLIP+ZipAF [44]	95.98	96.67	89.77	55.07	40.83	76.84	76.22	71.11	29.58	22.37	95.22	98.74	90.17	78.88	46.97
		NAGL+ZipAF [24]	97.14	96.75	93.24	59.49	42.52	85.71	79.49	79.15	42.42	32.07	97.94	99.07	92.72	75.30	49.40
		UniADC (CLIP)	98.57	98.55	91.42	85.57	50.01	92.74	84.98	82.15	64.40	35.86	99.35	99.19	94.48	93.91	49.94
		UniADC (DINO)	98.70	98.91	93.35	86.83	52.37	93.32	87.12	83.83	66.59	34.87	99.87	99.45	94.59	97.67	51.80

pler [51] with 1,000 original diffusion steps. The noise factor γ is uniformly sampled between 0.4 and 0.6, and the number of accelerated sampling steps is set to 10. For mask generation, we leverage BiRefNet [52] for binary segmentation to ensure that the mask is located within the foreground region. We set the mini-batch size to 32 for category consistency selection, and generate 16 samples with a resolution of 512×512 per anomaly category for discriminator training. For the implicit-normal discriminator, we adopt two experimental settings, namely **UniADC (CLIP)** and **UniADC (DINO)**, which use the CLIP ViT-L/14 [53] and the DINOv3-based `dino.txt` [54] as the vision-language backbone of the discriminator, respectively. We set both the anomaly score threshold τ and the loss weight λ to 0.5. The list of anomaly priors is provided in the *Supplementary Material*.

3) *Metrics*. We use the Area Under the Receiver Operating Characteristic Curve (I-AUC) metric to evaluate image-level anomaly detection performance. For pixel-level anomaly location, we use Pixel-AUROC (P-AUC) and Per Region Overlap (PRO) [55] metrics. In addition, we report the Top-1 classification accuracy (Acc) and Mean Intersection over Union (mIoU) to evaluate image-level and pixel-level anomaly classification performance, respectively. For the ‘‘combined’’ category in MVTec-FS dataset [5], we only evaluate its anomaly detection performance and exclude it from the anomaly classification metrics, as in previous works [5], [6].

4) *Baselines*. In the zero-shot setting, we adopt InCTRL [47], PatchCore [17], AnomalyDINO [48], PromptAD [8], AnomalyGPT [9], and WinCLIP [7] as baseline methods. For AnomalyGPT [9], we cast classification as a single-choice QA task by prompting the model with candidate anomaly types. For WinCLIP [7], we provide it with anomaly category

descriptions and compute the similarity between patch features and anomaly category embeddings, obtaining the anomaly classification results. In the few-shot setting, we combine anomaly detection methods such as PatchCore [17], WinCLIP [7], PromptAD [8], AnomalyCLIP [44], and NAGL [24] with the anomaly classification method ZipAF [5] as our baseline methods. We employ the threshold selection strategy proposed in AnomalyNCD [6] to determine the anomaly score threshold, and fine-tune PromptAD [8] and AnomalyCLIP [44] using few-shot anomaly samples to enhance their anomaly detection performance. To ensure a fair comparison, the visual backbones of CLIP- and DINO-based methods are kept consistent with **UniADC (CLIP)** and **UniADC (DINO)**, respectively.

B. Experimental Results

1) *Anomaly Detection and Classification Results*. Tables II and III report the anomaly detection and classification results under zero-shot and few-shot settings, respectively. In the zero-shot setting, most baselines struggle to identify specific anomaly categories due to the absence of real anomaly samples. Although some methods incorporate Vision-Language Models (VLMs) or Large Language Models (LLMs) with anomaly priors, they still fail to achieve satisfactory performance. In contrast, UniADC fully exploits the relevance between anomaly detection and classification, thereby achieving promising performance in both tasks. Compared to other methods, it achieves approximately a 20% improvement in classification accuracy and a 10% improvement in mIoU. Moreover, **UniADC (DINO)** achieves superior detection and classification accuracy over **UniADC (CLIP)**, highlighting the remarkable performance of DINOv3 [54] in extracting fine-grained image features. In the few-shot setting, UniADC deliv-

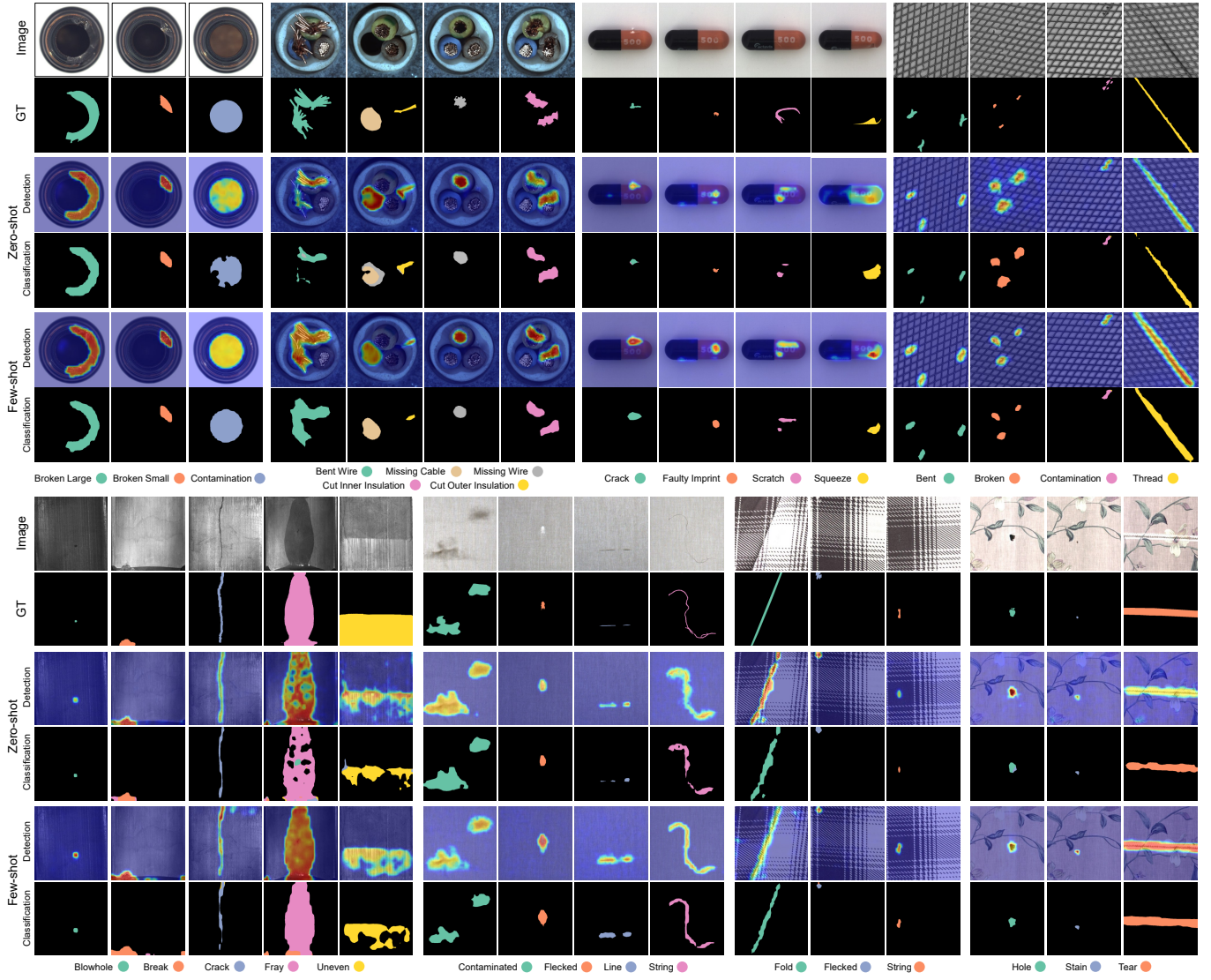


Fig. 7. Qualitative results of UniADC on the MVTec-FS, MTD, and WFDD datasets under zero-shot ($K_n=2$) and few-shot ($K_n=2, K_a=1$) settings.

ers substantial performance gains, even with only one anomaly sample per category, demonstrating its low cost and effective data utilization. Furthermore, it markedly outperforms other two-stage methods, showcasing the benefit of unifying anomaly detection and classification. Qualitative results in Fig. 7 further illustrate its ability to accurately localize and classify anomalous regions under various settings, emphasizing its strong generalization capability and practical applicability.

2) *Experimental Results with Full-shot Normal Samples.* In addition, UniADC can be extended to the setting of full-shot normal samples, with the results provided in Table IV. We use the unsupervised anomaly detection methods PatchCore [17], RD4AD [56], and RealNet [34], as well as the semi-supervised method BGAD [23], in combination with the anomaly classification method ZipAF [5] as our baselines. When sufficient normal samples are available, UniADC can achieve anomaly detection performance comparable to mainstream full-shot methods. Moreover, it significantly improves anomaly classification performance, addressing the limitations

TABLE IV
COMPARISON OF UNIADC WITH ALTERNATIVE METHODS ON THE MVTEC-FS DATASET USING FULL-SHOT NORMAL SAMPLES, WITH $K_a = 1$.

Method	Detection			Classification	
	I-AUC	P-AUC	PRO	Acc	mIoU
PatchCore+ZipAF [17]	98.77	98.76	95.17	69.50	39.60
RD4AD+ZipAF [56]	98.89	98.54	94.23	62.23	39.76
RealNet+ZipAF [34]	99.60	99.02	93.71	67.20	43.24
BGAD+ZipAF [23]	98.80	98.24	92.33	65.62	41.93
UniADC (CLIP)	98.85	98.73	93.76	87.01	51.59
UniADC (DINO)	99.41	98.95	94.06	87.86	51.93

of existing approaches in this aspect and demonstrating its unique practical value.

3) *Experimental Results on Anomaly Synthesis.* Table V presents the performance of UniADC and other anomaly synthesis methods in terms of anomaly detection, classification, and the quality of synthetic anomaly images. For the zero-

TABLE V
COMPARISON OF UNIADC WITH OTHER ANOMALY SYNTHESIS METHODS ON THE MVTEC-FS DATASET, USING DINOv3 AS THE VISION BACKBONE.

Setting	Method	Detection			Classification		Image Quality	
		I-AUC	P-AUC	PRO	Acc	mIoU	IS \uparrow	IC-L \uparrow
Zero-shot ($K_n = 2$)	CutPaste [30]	94.15	92.60	78.31	-	-	1.35	0.11
	NSA [31]	95.06	93.70	77.20	-	-	1.50	0.14
	DRÆM [43]	95.90	95.71	84.48	-	-	1.53	0.16
	RealNet [34]	95.83	96.11	85.76	-	-	1.58	0.14
	AnomalyAny [35]	96.08	95.78	88.15	54.07	25.46	1.65	0.18
	UniADC	97.09	97.04	92.15	74.74	36.66	1.70	0.21
Few-shot ($K_n = 2, K_a = 1$)	<i>w/o Synthesis</i>	96.28	97.45	84.84	77.40	42.23	-	-
	<i>CutPasteByMask</i>	97.38	98.00	88.96	82.41	47.07	1.35	0.07
	AnoGen [22]	97.69	98.52	88.79	85.74	50.34	1.39	0.15
	DualAnoDiff [39]	96.50	98.47	89.62	85.61	50.71	1.48	0.26
	AnomalyDiffusion [38]	97.16	98.21	90.16	83.07	50.82	1.50	0.21
	UniADC	98.56	98.90	92.48	86.85	51.49	1.75	0.24

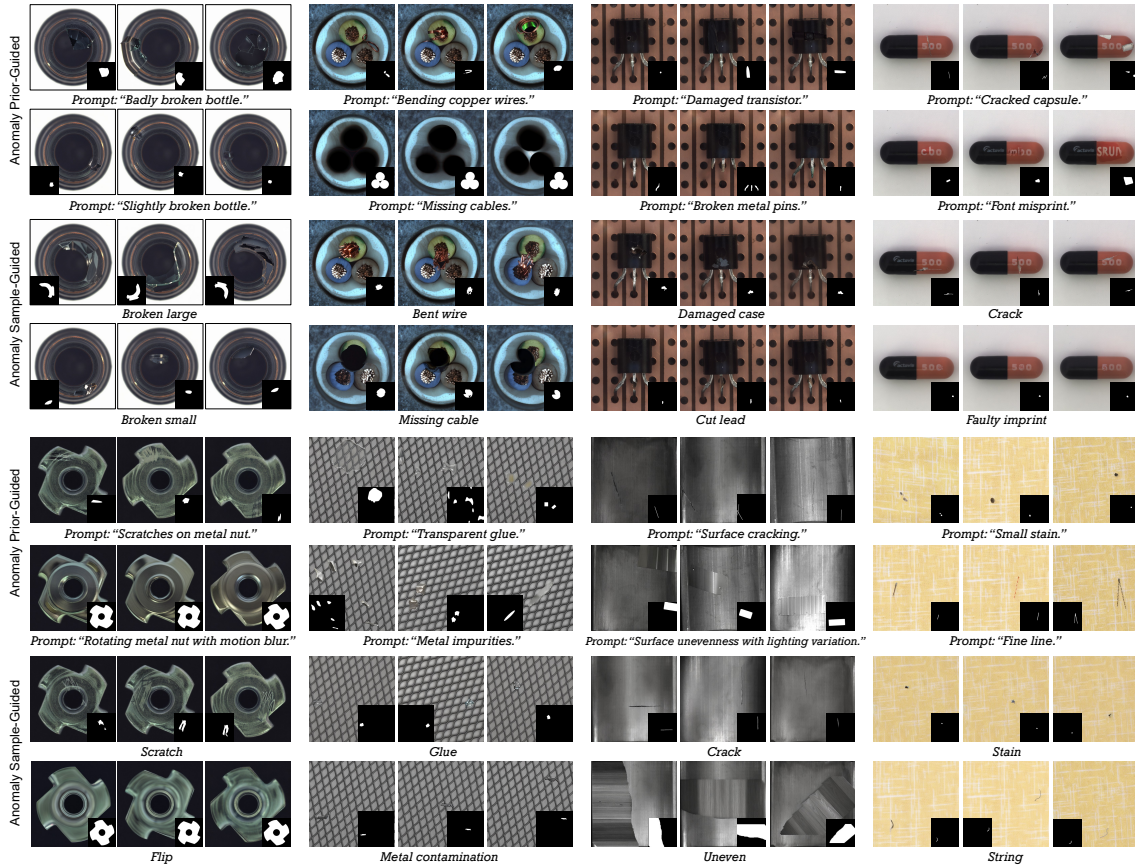


Fig. 8. Examples of synthetic anomaly samples generated by UniADC under the guidance of anomaly prior and anomaly sample on the MVTEc-FS, MTD, and WFDD datasets.

shot setting, we use CutPaste [30], NSA [31], DRÆM [43], RealNet [34], and AnomalyAny [35] as baseline methods. For the few-shot setting, we use AnoGen [22], DualAnoDiff [39], AnomalyDiffusion [38], as well as the methods without anomaly synthesis (*w/o Synthesis*) and CutPaste based on masks (*CutPasteByMask*) as our baseline methods. We use the synthetic anomaly samples from the above methods to train the implicit-normal discriminator and evaluate their quality using the IS and IC-LPIPS metrics, as in previous works [38], [39]. In both settings, UniADC achieves satisfactory performance and outperforms other methods in multiple aspects. Compared

to *w/o Synthesis* and *CutPasteByMask*, UniADC shows significant performance improvements, demonstrating the necessity of anomaly sample augmentation and image inpainting. Fig. 8 presents synthetic anomaly samples generated by UniADC. By incorporating an inpainting control network and reliable category consistency selection strategies, UniADC can generate high-quality anomaly samples that are mask-consistent, category-aligned, and visually diverse. These properties enable UniADC to generalize well across a wide range of anomaly detection and classification scenarios.

4) *Open-set Anomaly Detection and Classification*. For

TABLE VI
COMPARISON OF UNIADC PERFORMANCE ON THE *Hazelnut* CLASS OF MVTEC-FS DATASET UNDER OPEN- AND CLOSED-SET SETTINGS, USING DINOv3 AS THE VISION BACKBONE.

Setting	I-AUC	P-AUC	PRO	Acc (seen)				
				Normal	Crack	Cut	Hole	AVG
Closed-set	99.63	97.53	91.29	97.50	55.56	62.50	88.89	86.36
Open-set	99.41	99.09	95.21	95.00	44.44	62.50	88.89	83.33

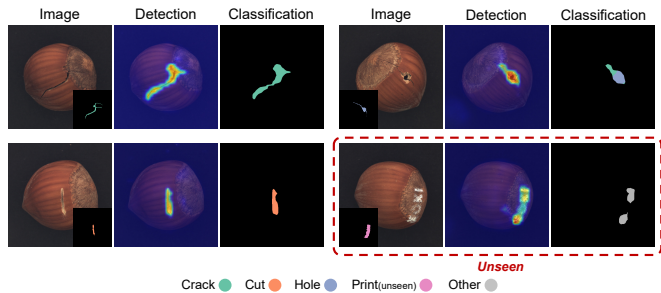


Fig. 9. Qualitative results of UniADC under the setting of open-set anomaly detection and classification.

open-set anomaly detection, a model is trained on only a subset of anomaly types and is expected to generalize to detect unseen anomalies [57]. We extend this setting to anomaly detection and classification, where a model is designed to detect both seen and unseen anomalies while ensuring correct classification of the seen anomalies. We propose a simple yet effective approach to adapt UniADC for open-set anomaly detection and classification tasks. Specifically, during training, we use unconstrained anomaly synthesis methods (e.g., DRÆM [43]) to generate class-agnostic anomalous images and align them with an additional learnable anomaly embedding. During inference, the learnable embedding is used to match all unseen anomaly types and categorize them as “Other”.

We conducted experiments on the *Hazelnut* class of the MVTEC-FS dataset [5] to validate the effectiveness of our proposed approach. We use “Crack”, “Cut”, and “Hole” as seen anomalies, and “Print” as the unseen anomaly. We adopt the zero-shot setting ($K_n = 2$), where no prior knowledge about the “Print” category is provided during training. Table VI presents the anomaly detection and classification results of UniADC under both open-set and closed-set settings. In the open-set setting, UniADC achieves anomaly detection and classification performance comparable to the closed-set, demonstrating that it generalizes well to unseen anomalies while avoiding their interference with anomaly classification. Fig. 9 presents qualitative results of UniADC, showing that it ensures accurate detection and classification of seen anomalies, while aligning unseen anomalies with the learnable anomaly embedding to identify them as the “Other” type.

5) More qualitative results and per-class metrics can be found in the *Supplementary Material*.

C. Ablation Study

We conducted extensive experiments to validate the effectiveness of each component in UniADC and its hyperparameter

TABLE VII
ABLATION RESULTS OF UNIADC ON THE MVTEC-FS DATASET. \mathcal{L}_{CE} DENOTES THE CROSS-ENTROPY LOSS, IND DENOTES THE IMPLICIT-NORMAL DISCRIMINATOR, AND CCS REFERS TO THE CATEGORY CONSISTENCY SELECTION STRATEGY.

Setting	Component	I-AUC	P-AUC	PRO	Acc	mIoU
Zero-shot ($K_n = 2$)	w/o \mathcal{L}_{CE}	97.76 _(0.67)	96.23 _(0.81)	87.10 _(5.05)	-	-
	w/o IND	96.72 _(0.37)	95.70 _(1.34)	91.44 _(0.71)	55.91 _(18.83)	24.99 _(11.67)
	w/o CCS	95.19 _(1.90)	96.02 _(1.02)	89.26 _(2.89)	66.16 _(8.58)	33.15 _(3.51)
	UniADC	97.09	97.04	92.15	74.74	36.66
Few-shot ($K_n = 2, K_a = 1$)	w/o \mathcal{L}_{CE}	97.76 _(0.80)	98.33 _(0.57)	86.26 _(6.22)	-	-
	w/o IND	97.27 _(1.29)	96.92 _(1.98)	92.37 _(0.11)	60.04 _(26.81)	30.33 _(21.16)
	w/o CCS	96.84 _(1.72)	98.08 _(0.82)	88.56 _(3.92)	79.91 _(6.94)	45.37 _(6.12)
	UniADC	98.56	98.90	92.48	86.85	51.49

TABLE VIII
ABLATION STUDY OF ANOMALY PRIOR ON THE MVTEC-FS DATASET WITH $K_n = 2$.

Description	Shape	Size	I-AUC	P-AUC	PRO	Acc	mIoU
×	×	×	96.04	95.82	88.22	65.31	31.76
✓	×	×	96.75	96.24	91.03	69.58	34.54
×	✓	×	96.28	96.00	89.86	66.02	32.56
×	×	✓	96.49	96.29	90.69	67.08	33.26
✓	✓	×	96.97	96.56	91.73	70.84	34.79
✓	×	✓	97.12	96.80	91.58	72.69	35.17
✓	✓	✓	97.09	97.04	92.15	74.74	36.66

sensitivity. By default, all ablation experiments use DINOv3 [54] as the backbone of the discriminator.

1) *Ablation Study on UniADC Components*. Table VII investigates the impact of various UniADC components on its performance. When the anomaly classification loss is removed, UniADC degenerates into a standard anomaly detection model. In the zero-shot setting, image-level anomaly detection performance improves slightly, while anomaly localization performance degrades. In the few-shot setting, all metrics decline, indicating that incorporating the anomaly classification task does not compromise anomaly detection but rather enhances the robustness and accuracy of anomaly detection. In the absence of the implicit-normal discriminator, we follow [26] to directly align image patch features with the normal class and Y anomaly classes (totaling $Y + 1$ classes), while employing Focal Loss [45] to mitigate pixel distribution imbalance. However, the model experiences a substantial performance decline, with anomaly classification accuracy dropping by approximately 20%. This significant degradation underscores the necessity of implicitly modeling the normal class. Moreover, UniADC exhibits consistent performance improvement across all settings with the integration of category consistency selection, highlighting its critical role in enhancing the quality of synthesized anomaly samples.

2) *Ablation Study on Anomaly Prior*. Table VIII investigates the impact of different types of anomaly priors on the performance of UniADC. The experimental results show that anomaly descriptions have the most significant impact on the performance of UniADC, especially in anomaly classification. For most anomaly categories, the anomaly description is a

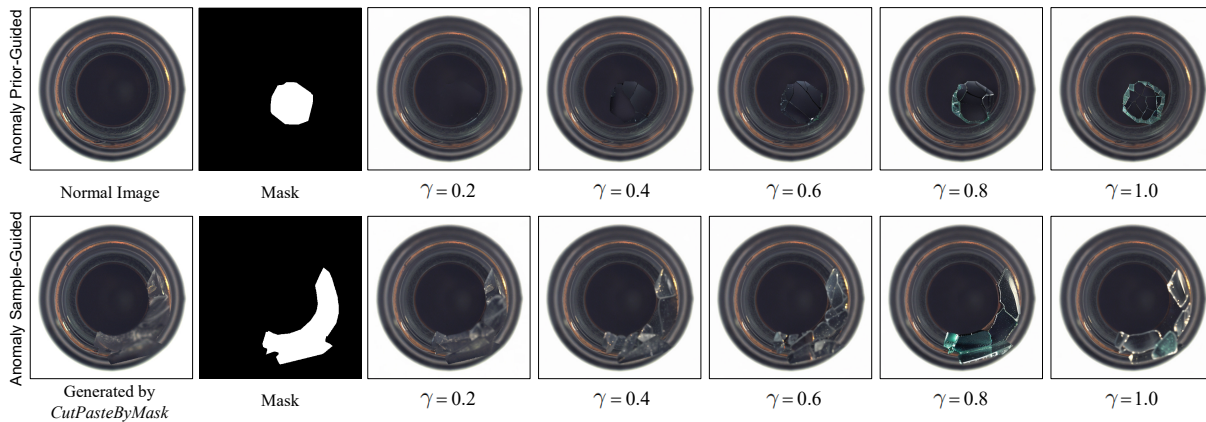


Fig. 10. Examples of synthetic anomaly images generated by UniADC across different noise factors, guided by anomaly prior or anomaly sample, respectively.

TABLE IX
ABLATION STUDY OF THE NOISE FACTOR ON THE MVTEC-FS DATASET.

Setting	γ	I-AUC	P-AUC	PRO	Acc	mIoU
Zero-shot ($K_n = 2$)	(0, 0.2]	93.19	95.76	85.43	61.46	30.89
	(0.2, 0.4]	96.35	96.78	91.03	73.67	36.84
	(0.4, 0.6]	97.09	97.04	92.15	74.74	36.66
	(0.6, 0.8]	97.14	96.65	91.58	74.40	35.81
	(0.8, 1.0]	96.83	96.38	90.38	72.91	34.83
Few-shot ($K_n = 2, K_a = 1$)	(0, 0.2]	97.85	98.53	90.86	84.44	49.34
	(0.2, 0.4]	98.69	98.71	91.92	85.89	50.85
	(0.4, 0.6]	98.56	98.90	92.48	86.85	51.49
	(0.6, 0.8]	98.42	98.84	92.18	86.54	51.55
	(0.8, 1.0]	98.21	98.77	88.95	85.03	50.40

TABLE X
ABLATION STUDY OF THE MINI-BATCH SIZE FOR CATEGORY CONSISTENCY SELECTION ON THE MVTEC-FS DATASET.

Setting	B	I-AUC	P-AUC	PRO	Acc	mIoU
Zero-shot ($K_n = 2$)	8	95.93	96.55	90.55	71.90	33.17
	16	96.29	96.80	90.38	73.12	35.14
	32	97.09	97.04	92.15	74.74	36.66
	64	97.07	96.98	92.47	74.91	36.98
Few-shot ($K_n = 2, K_a = 1$)	8	97.97	98.67	90.20	84.72	50.17
	16	98.04	98.72	90.49	85.94	50.63
	32	98.56	98.90	92.48	86.85	51.49
	64	99.02	98.70	92.81	86.93	51.12

synonym of its name or a combination of its name and the detection object, such as “Foreign matter in the bottle”. For a few anomaly categories, we introduce additional anomaly information, such as the color of the anomalous region, to aid in anomaly classification. A comprehensive list of these descriptions is provided in the *Supplementary Material*. When anomaly descriptions are unavailable, we simply use anomaly category names as prompts. The introduction of anomaly descriptions enables UniADC to achieve improvements of 4.27% in classification accuracy and 2.78% in mIoU. Compared to anomaly descriptions, shape and size priors are generally difficult to apply to certain types of anomalies. For example, it is hard to predetermine the shapes and sizes of anomaly types such as “Scratch” and “Crack”. Moreover, in our experiments, the size prior yields greater performance improvements for UniADC than the shape prior. When all three types of anomaly priors are applied, UniADC achieves the best overall performance.

3) *Ablation Study on Noise Factor*. Table IX presents the impact of the noise factor γ on the performance of UniADC. A larger γ increases the diversity of synthetic anomaly samples while also causing greater deviation from the original image distribution, as shown in Fig. 10, which may undermine UniADC’s ability to detect hard anomaly cases. Conversely, a smaller γ may result in synthetic anomaly samples that do not align well with the provided anomaly description, leading to false positive anomalies or limited diversity. In our

experiments, we uniformly sample γ between 0.4 and 0.6 to ensure a balance between quality and diversity.

4) *Ablation Study on Sampling Hyperparameters and Computational Efficiency Analysis*. Tables X and XI respectively present the ablation study results on the mini-batch size in category consistency selection and the number of synthetic anomaly samples. Increasing the mini-batch size and the number of synthetic samples can improve the quality and diversity of training data, thereby enhancing the performance of UniADC. However, this also significantly increases the training cost. To ensure the performance of UniADC while reducing computational cost, we set the mini-batch size and the number of synthetic anomaly samples to 32 and 16, respectively. We implement UniADC using PyTorch, and it takes approximately 35 seconds to generate an anomaly image on a single Nvidia RTX 4090 GPU. The average training time of UniADC (including anomaly sample synthesis and discriminator training) is about 1 GPU hour. During the inference stage, the anomaly synthesis process is omitted. The main computational overhead of UniADC lies in the forward pass of the vision-language backbone, and its inference speed is comparable to that of other VLM-based methods, such as AnomalyCLIP [44].

5) *Ablation Study on Anomaly Score Threshold*. Fig. 11 illustrates the effect of varying the anomaly score threshold on the anomaly classification performance of UniADC. Compared to other methods [7], [8], UniADC demonstrates improved robustness to threshold variations, consistently achieving reliable

TABLE XI
ABLATION STUDY OF THE NUMBER OF SYNTHETIC ANOMALY SAMPLES ON THE MVTEC-FS DATASET.

Setting	Number of Synthetic Samples	I-AUC	P-AUC	PRO	Acc	mIoU
Zero-shot ($K_n = 2$)	2	93.25	95.89	86.10	64.19	30.37
	4	95.99	96.13	88.75	69.63	33.20
	8	96.34	96.85	91.73	73.55	35.79
	16	97.09	97.04	92.15	74.74	36.66
	32	97.16	96.93	92.04	74.82	36.86
Few-shot ($K_n = 2, K_a = 1$)	2	97.25	98.05	87.90	83.05	46.70
	4	98.09	98.05	91.02	84.94	49.34
	8	98.27	98.16	91.53	85.59	51.03
	16	98.56	98.90	92.48	86.85	51.49
	32	98.72	98.75	92.20	86.94	51.80

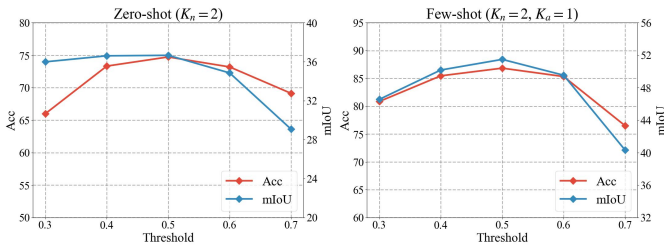


Fig. 11. Ablation study of the anomaly score threshold on the MVTEC-FS dataset.

performance when the threshold is set between 0.4 and 0.6, which simplifies the threshold selection process and improves practical feasibility. In our experiments, we simply fixed the threshold at 0.5.

V. CONCLUSION

This paper presents UniADC, a unified paradigm that integrates anomaly detection and classification into a cohesive generative-discriminative framework. By implicitly modeling the normal manifold, our approach effectively suppresses the inherent bias caused by pixel-level distribution imbalance, while the training-free controllable inpainting network maximizes data utility under extreme scarcity. The synergy between category-controllable anomaly synthesis and fine-grained feature alignment not only yields superior performance across multiple benchmarks but also provides a scalable solution for minimal-supervision scenarios. In future work, we aim to further enhance the versatility of our approach by extending its application to diverse domains, such as medical image anomaly detection and classification.

REFERENCES

- [1] X. Tao, X. Gong, X. Zhang, S. Yan, and C. Adak, "Deep learning for unsupervised anomaly localization in industrial images: A survey," *IEEE Transactions on Instrumentation and Measurement*, vol. 71, pp. 1–21, 2022.
- [2] X. Xia, X. Pan, N. Li, X. He, L. Ma, X. Zhang, and N. Ding, "Gan-based anomaly detection: A review," *Neurocomputing*, vol. 493, pp. 497–535, 2022.
- [3] J. Diers and C. Pigorsch, "A survey of methods for automated quality control based on images," *International Journal of Computer Vision*, vol. 131, no. 10, pp. 2553–2581, 2023.
- [4] J. Liu, G. Xie, J. Wang, S. Li, C. Wang, F. Zheng, and Y. Jin, "Deep industrial image anomaly detection: A survey," *Machine Intelligence Research*, vol. 21, no. 1, pp. 104–135, 2024.

- [5] S. Lyu, R. Zhang, Z. Ma, F. Liao, D. Mo, and W. Wong, "Mvrec: A general few-shot defect classification model using multi-view region-context," in *Proceedings of the AAAI Conference on Artificial Intelligence*, vol. 39, no. 6, 2025, pp. 5937–5945.
- [6] Z. Huang, X. Li, H. Liu, F. Xue, Y. Wang, and Y. Zhou, "Anomalyncd: Towards novel anomaly class discovery in industrial scenarios," in *Proceedings of the Computer Vision and Pattern Recognition Conference*, 2025, pp. 4755–4765.
- [7] J. Jeong, Y. Zou, T. Kim, D. Zhang, A. Ravichandran, and O. Dabeer, "Winclip: Zero-few-shot anomaly classification and segmentation," in *Proceedings of the IEEE/CVF Conference on Computer Vision and Pattern Recognition*, 2023, pp. 19 606–19 616.
- [8] X. Li, Z. Zhang, X. Tan, C. Chen, Y. Qu, Y. Xie, and L. Ma, "Promptad: Learning prompts with only normal samples for few-shot anomaly detection," in *Proceedings of the IEEE/CVF Conference on Computer Vision and Pattern Recognition*, 2024, pp. 16 838–16 848.
- [9] Z. Gu, B. Zhu, G. Zhu, Y. Chen, M. Tang, and J. Wang, "Anomalygpt: Detecting industrial anomalies using large vision-language models," in *Proceedings of the AAAI conference on artificial intelligence*, vol. 38, no. 3, 2024, pp. 1932–1940.
- [10] F. Tao, G.-S. Xie, F. Zhao, and X. Shu, "Kernel-aware graph prompt learning for few-shot anomaly detection," in *Proceedings of the AAAI Conference on Artificial Intelligence*, vol. 39, no. 7, 2025, pp. 7347–7355.
- [11] X. Zhang, M. Xu, D. Qiu, R. Yan, N. Lang, and X. Zhou, "Medi-clip: Adapting clip for few-shot medical image anomaly detection," in *International Conference on Medical Image Computing and Computer-Assisted Intervention*. Springer, 2024, pp. 458–468.
- [12] C. Huang, A. Jiang, J. Feng, Y. Zhang, X. Wang, and Y. Wang, "Adapting visual-language models for generalizable anomaly detection in medical images," in *Proceedings of the IEEE/CVF Conference on Computer Vision and Pattern Recognition*, 2024, pp. 11 375–11 385.
- [13] R. Rombach, A. Blattmann, D. Lorenz, P. Esser, and B. Ommer, "High-resolution image synthesis with latent diffusion models," in *Proceedings of the IEEE/CVF conference on computer vision and pattern recognition*, 2022, pp. 10 684–10 695.
- [14] L. Zhang, A. Rao, and M. Agrawala, "Adding conditional control to text-to-image diffusion models," in *Proceedings of the IEEE/CVF international conference on computer vision*, 2023, pp. 3836–3847.
- [15] Y. Huang, C. Qiu, and K. Yuan, "Surface defect saliency of magnetic tile," *The Visual Computer*, vol. 36, no. 1, pp. 85–96, 2020.
- [16] Q. Chen, H. Luo, C. Lv, and Z. Zhang, "A unified anomaly synthesis strategy with gradient ascent for industrial anomaly detection and localization," in *European Conference on Computer Vision*. Springer, 2024, pp. 37–54.
- [17] K. Roth, L. Pemula, J. Zepeda, B. Schölkopf, T. Brox, and P. Gehler, "Towards total recall in industrial anomaly detection," in *Proceedings of the IEEE/CVF conference on computer vision and pattern recognition*, 2022, pp. 14 318–14 328.
- [18] T. Defard, A. Setkov, A. Loesch, and R. Audigier, "Padim: a patch distribution modeling framework for anomaly detection and localization," in *International Conference on Pattern Recognition*. Springer, 2021, pp. 475–489.
- [19] G. Wang, Y. Zou, S. He, Y. Wang, and R. Dai, "Anomaly detection and localization via reverse distillation with latent anomaly suppression," *IEEE Transactions on Circuits and Systems for Video Technology*, 2025.
- [20] W. Luo, P. Xing, Y. Cao, H. Yao, W. Shen, and Z. Li, "Ura-net: Uncertainty-integrated anomaly perception and restoration attention network for unsupervised anomaly detection," *IEEE Transactions on Circuits and Systems for Video Technology*, 2025.
- [21] X. Zhang, M. Xu, and X. Zhou, "Towards high-resolution industrial image anomaly detection," *arXiv preprint arXiv:2508.12931*, 2025.
- [22] G. Gui, B.-B. Gao, J. Liu, C. Wang, and Y. Wu, "Few-shot anomaly-driven generation for anomaly classification and segmentation," in *European Conference on Computer Vision*. Springer, 2024, pp. 210–226.
- [23] X. Yao, R. Li, J. Zhang, J. Sun, and C. Zhang, "Explicit boundary guided semi-push-pull contrastive learning for supervised anomaly detection," in *Proceedings of the IEEE/CVF Conference on Computer Vision and Pattern Recognition*, 2023, pp. 24 490–24 499.
- [24] Y. Wang, X. Wang, Y. Gong, and J. XIAO, "Normal-abnormal guided generalist anomaly detection," in *The Thirty-ninth Annual Conference on Neural Information Processing Systems*, 2025.
- [25] Z. Sun, Y. Fang, T. Wu, P. Zhang, Y. Zang, S. Kong, Y. Xiong, D. Lin, and J. Wang, "Alpha-clip: A clip model focusing on wherever you want," in *Proceedings of the IEEE/CVF conference on computer vision and pattern recognition*, 2024, pp. 13 019–13 029.

- [26] Y. Sadikaj, H. Zhou, L. Halilaj, S. Schmid, S. Staab, and C. Plant, "Multi-tasks: Defect-aware supervision for multi-type anomaly detection and segmentation in zero-shot learning," in *Proceedings of the IEEE/CVF International Conference on Computer Vision*, 2025, pp. 22 978–22 988.
- [27] K. Song and Y. Yan, "A noise robust method based on completed local binary patterns for hot-rolled steel strip surface defects," *Applied Surface Science*, vol. 285, pp. 858–864, 2013.
- [28] Z. Zhan, J. Zhou, and B. Xu, "Fabric defect classification using prototypical network of few-shot learning algorithm," *Computers in Industry*, vol. 138, p. 103628, 2022.
- [29] Z. Lai, Y. Lu, X. Li, J. Lin, Y. Qu, L. Cao, M. Li, and R. Ji, "Anomaly-painter: Vision-language-diffusion synergy for zero-shot realistic and diverse industrial anomaly synthesis," *arXiv preprint arXiv:2503.07253*, 2025.
- [30] C.-L. Li, K. Sohn, J. Yoon, and T. Pfister, "Cutpaste: Self-supervised learning for anomaly detection and localization," in *Proceedings of the IEEE/CVF conference on computer vision and pattern recognition*, 2021, pp. 9664–9674.
- [31] H. M. Schlüter, J. Tan, B. Hou, and B. Kainz, "Natural synthetic anomalies for self-supervised anomaly detection and localization," in *European Conference on Computer Vision*. Springer, 2022, pp. 474–489.
- [32] P. Xing, Y. Sun, D. Zeng, and Z. Li, "Normal image guided segmentation framework for unsupervised anomaly detection," *IEEE Transactions on Circuits and Systems for Video Technology*, vol. 34, no. 6, pp. 4639–4652, 2023.
- [33] T. D. Tien, A. T. Nguyen, N. H. Tran, T. D. Huy, S. Duong, C. D. T. Nguyen, and S. Q. Truong, "Revisiting reverse distillation for anomaly detection," in *Proceedings of the IEEE/CVF conference on computer vision and pattern recognition*, 2023, pp. 24 511–24 520.
- [34] X. Zhang, M. Xu, and X. Zhou, "Realnet: A feature selection network with realistic synthetic anomaly for anomaly detection," in *Proceedings of the IEEE/CVF conference on computer vision and pattern recognition*, 2024, pp. 16 699–16 708.
- [35] H. Sun, Y. Cao, H. Dong, and O. Fink, "Unseen visual anomaly generation," in *Proceedings of the Computer Vision and Pattern Recognition Conference*, 2025, pp. 25 508–25 517.
- [36] Y. Jiang, W. Luo, H. Zhang, Q. Chen, H. Yao, W. Shen, and Y. Cao, "Anomagic: Crossmodal prompt-driven zero-shot anomaly generation," *arXiv preprint arXiv:2511.10020*, 2025.
- [37] Y. Duan, Y. Hong, L. Niu, and L. Zhang, "Few-shot defect image generation via defect-aware feature manipulation," in *Proceedings of the AAAI conference on artificial intelligence*, vol. 37, no. 1, 2023, pp. 571–578.
- [38] T. Hu, J. Zhang, R. Yi, Y. Du, X. Chen, L. Liu, Y. Wang, and C. Wang, "Anomalydiffusion: Few-shot anomaly image generation with diffusion model," in *Proceedings of the AAAI conference on artificial intelligence*, vol. 38, no. 8, 2024, pp. 8526–8534.
- [39] Y. Jin, J. Peng, Q. He, T. Hu, J. Wu, H. Chen, H. Wang, W. Zhu, M. Chi, J. Liu *et al.*, "Dual-interrelated diffusion model for few-shot anomaly image generation," in *Proceedings of the Computer Vision and Pattern Recognition Conference*, 2025, pp. 30 420–30 429.
- [40] J. Song, D. Park, K. Baek, S. Lee, J. Choi, E. Kim, and S. Yoon, "Defectfill: Realistic defect generation with inpainting diffusion model for visual inspection," in *Proceedings of the Computer Vision and Pattern Recognition Conference*, 2025, pp. 18 718–18 727.
- [41] X. Ju, X. Liu, X. Wang, Y. Bian, Y. Shan, and Q. Xu, "Brushnet: A plug-and-play image inpainting model with decomposed dual-branch diffusion," in *European Conference on Computer Vision*. Springer, 2024, pp. 150–168.
- [42] Z. Wang, A. C. Bovik, H. R. Sheikh, and E. P. Simoncelli, "Image quality assessment: from error visibility to structural similarity," *IEEE transactions on image processing*, vol. 13, no. 4, pp. 600–612, 2004.
- [43] V. Zavrtanik, M. Kristan, and D. Skočaj, "Draem-a discriminatively trained reconstruction embedding for surface anomaly detection," in *Proceedings of the IEEE/CVF international conference on computer vision*, 2021, pp. 8330–8339.
- [44] Q. Zhou, G. Pang, Y. Tian, S. He, and J. Chen, "AnomalyCLIP: Object-agnostic prompt learning for zero-shot anomaly detection," in *The Twelfth International Conference on Learning Representations*, 2024.
- [45] T.-Y. Lin, P. Goyal, R. Girshick, K. He, and P. Dollár, "Focal loss for dense object detection," in *Proceedings of the IEEE international conference on computer vision*, 2017, pp. 2980–2988.
- [46] F. Milletari, N. Navab, and S.-A. Ahmadi, "V-net: Fully convolutional neural networks for volumetric medical image segmentation," in *2016 fourth international conference on 3D vision (3DV)*. Ieee, 2016, pp. 565–571.
- [47] J. Zhu and G. Pang, "Toward generalist anomaly detection via in-context residual learning with few-shot sample prompts," in *Proceedings of the IEEE/CVF conference on computer vision and pattern recognition*, 2024, pp. 17 826–17 836.
- [48] S. Damm, M. Laszkiewicz, J. Lederer, and A. Fischer, "Anomalydino: Boosting patch-based few-shot anomaly detection with dinov2," in *2025 IEEE/CVF Winter Conference on Applications of Computer Vision (WACV)*. IEEE, 2025, pp. 1319–1329.
- [49] P. Bergmann, M. Fauser, D. Sattlegger, and C. Steger, "Mvtec-ad: A comprehensive real-world dataset for unsupervised anomaly detection," in *Proceedings of the IEEE/CVF conference on computer vision and pattern recognition*, 2019, pp. 9592–9600.
- [50] Y. Zou, J. Jeong, L. Pemula, D. Zhang, and O. Dabeer, "Spot-the-difference self-supervised pre-training for anomaly detection and segmentation," in *European Conference on Computer Vision*. Springer, 2022, pp. 392–408.
- [51] J. Song, C. Meng, and S. Ermon, "Denoising diffusion implicit models," in *International Conference on Learning Representations*, 2021.
- [52] P. Zheng, D. Gao, D.-P. Fan, L. Liu, J. Laaksonen, W. Ouyang, and N. Sebe, "Bilateral reference for high-resolution dichotomous image segmentation," *CAAI Artificial Intelligence Research*, vol. 3, p. 9150038, 2024.
- [53] A. Radford, J. W. Kim, C. Hallacy, A. Ramesh, G. Goh, S. Agarwal, G. Sastry, A. Askell, P. Mishkin, J. Clark *et al.*, "Learning transferable visual models from natural language supervision," in *International conference on machine learning*. PmlR, 2021, pp. 8748–8763.
- [54] O. Siméoni, H. V. Vo, M. Seitzer, F. Baldassarre, M. Oquab, C. Jose, V. Khalidov, M. Szafraniec, S. Yi, M. Ramamonjisoa *et al.*, "Dinov3," *arXiv preprint arXiv:2508.10104*, 2025.
- [55] P. Bergmann, M. Fauser, D. Sattlegger, and C. Steger, "Uninformed students: Student-teacher anomaly detection with discriminative latent embeddings," in *Proceedings of the IEEE/CVF conference on computer vision and pattern recognition*, 2020, pp. 4183–4192.
- [56] H. Deng and X. Li, "Anomaly detection via reverse distillation from one-class embedding," in *Proceedings of the IEEE/CVF conference on computer vision and pattern recognition*, 2022, pp. 9737–9746.
- [57] C. Ding, G. Pang, and C. Shen, "Catching both gray and black swans: Open-set supervised anomaly detection," in *Proceedings of the IEEE/CVF conference on computer vision and pattern recognition*, 2022, pp. 7388–7398.

TABLE S1
ANOMALY PRIOR LIST PROVIDED FOR EACH ANOMALY CATEGORY.

Dataset	Image Class	Anomaly Category	Description	Shape	Size	Dataset	Image Class	Anomaly Category	Description	Shape	Size	
MVTec-FS	Bottle	Broken large	Badly broken bottle		Large	MVTec-FS	Screw	Manipulated front	Damaged screw tip			
		Broken small	Slightly broken bottle		Small			Scratch head	Damaged screw head			
		Contamination	Foreign matter in the bottle					Scratch neck	Damaged screw neck			
	Cable	Bent wire	Bending copper wires					Thread side	Screw thread stripping			
		Cable swap	Cable swap	Foreground				Thread top	Damaged screw thread			
		Cut inner insulation	Cracks in the internal insulation				Tile	Crack	Cracks on the tile			
		Cut outer insulation	Cracks in the external insulation					Glue strip	Transparent glue			
		Missing cable	Missing cables	Foreground				Gray stroke	Gray-black stain		Large	
		Missing wire	Missing wires					Oil	Oil stain			
		Poke insulation	Puncture-induced holes				Rough	Rough white tile		Large		
	Capsule	Crack	Cracked capsule				Toothbrush	Defective	Missing bristles, Bending bristle, Foreign matter, A piece of thread			
		Faulty imprint	Font misprint, Font error						Transistor	Bent lead	Bending metal pins	
		Poke	A tiny hole on the capsule	Ellipse	Small		Cut lead	Broken metal pins				
		Scratch	Slight scratches on the capsule				Damaged case	Damaged transistor				
	Carpet	Squeeze	A capsule deformed by squeezing		Large		Wood	Color	Red stain, Black stain			
		Color	Red stain, Black stain						Hole	Hole in wood	Ellipse	
		Cut	A tiny cut in carpet						Liquid	Transparent liquid stains		
		Hole	Hole	Ellipse					Scratch	Scratches in wood		
		Metal contamination	Metal impurities, Metal foreign matter				Zipper	Broken teeth	Damage to the zipper			
	Thread	A piece of thread	Line, Hollow Ellipse	Small, Medium	Fabric border				Border damage of fabric			
	Grid	Bent	Bending metal grid						Fabric interior	Interior damage of fabric		
		Broken	Broken defect						Rough	Wear on the zipper		
		Glue	Transparent glue						Split teeth	Unzipped zipper		
		Metal contamination	Metal impurities, Metal foreign matter				Squeezed teeth	Squeezed zipper				
		Thread	A piece of thread	Line, Hollow Ellipse	Small, Medium		WFDD	Grey Cloth	Contaminated	Black stain		
	Hazelnut	Crack	A hazelnut with cracks						Flecked	White spot	Ellipse	Small
		Cut	A hazelnut with cutting marks						Line	Black linear stain	Line	Small
		Hole	A hazelnut with a hole	Ellipse					String	Fine line		Small
		Print	A hazelnut with printed text					Grid Cloth	Fold	Fabric with fold marks	Line	
	Leather	Color	Red stain, Black stain						Flecked	White spot	Ellipse	Small
		Cut	A tiny cut in leather					String	Fine line		Small	
		Fold	Fold marks in leather					Pink Flower	Hole	Hole	Ellipse	
		Glue	Transparent glue						Stain	Small stain		Small
	Poke	A puncture-induced hole	Ellipse	Small	Tear			Zipper-like tear				
	Metal Nut	Bent	Cracked metal nut					Yellow cloth	Fold	Fabric with fold marks	Line	
		Color	Red stain, Black stain						Stain	Small stain		Small
		Flip	Rotating metal nut with motion blur	Foreground					String	Fine line		Small
		Scratch	Scratches on metal nut						MTD	Blowhole	Black hole	Ellipse
	Pill	Color	Red stain, Black stain					Break		Surface crumpling		Small
		Contamination	Foreign matter on the pill					Crack		Surface cracking		Small
		Crack	Edge damage of the pill				Fray	Surface abrasion			Large	
		Faulty imprint	Font misprint, Font error				Uneven	Surface unevenness with lighting variation				
		Pill type	Mold growth on the pill	Foreground								Large
	Scratch	Scratches on the pill										

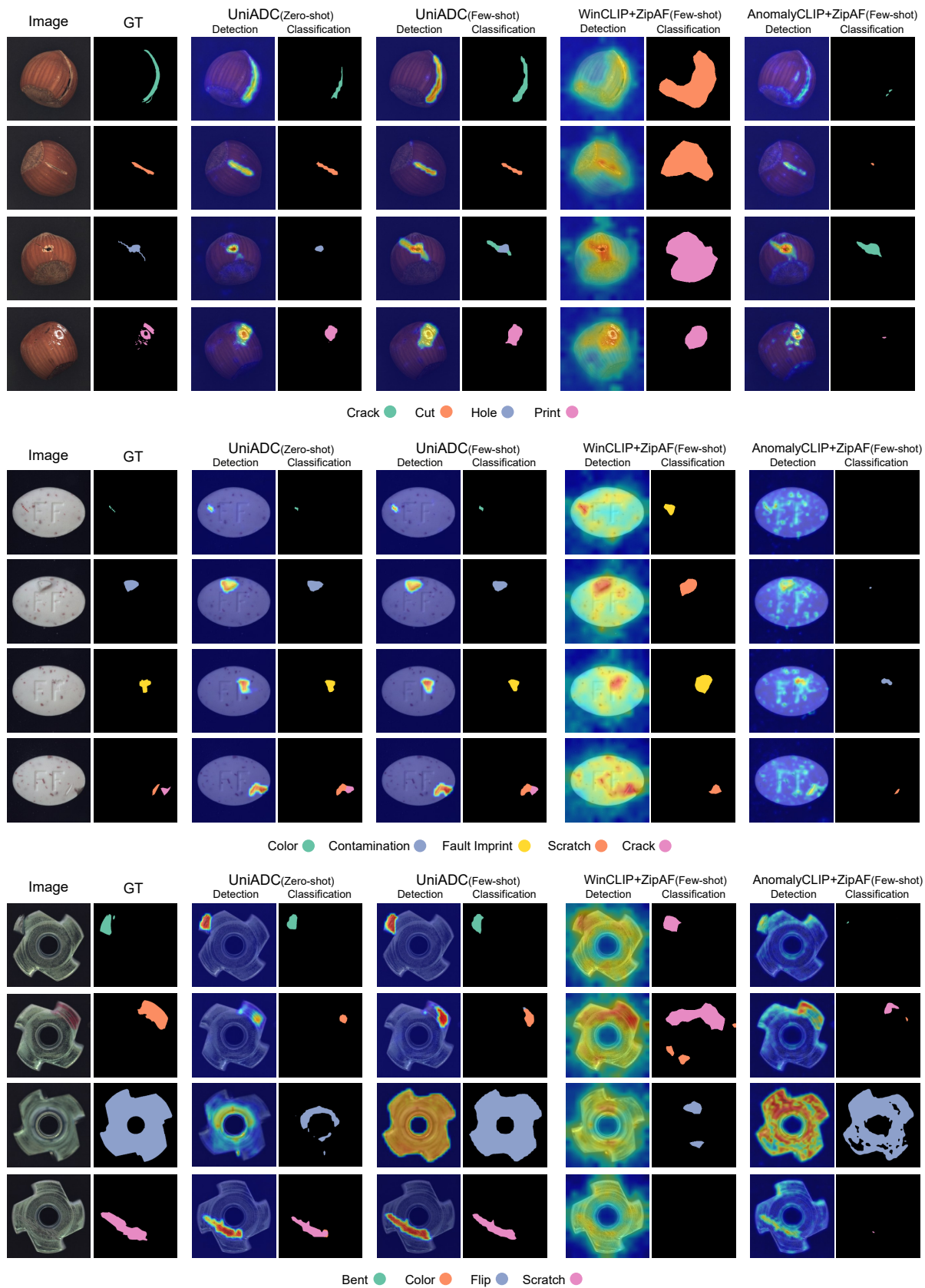


Fig. S1. Qualitative comparison of UniADC and other methods on the *Hazelnut*, *Pill*, and *Metal Nut* classes of the MVTec-FS dataset.

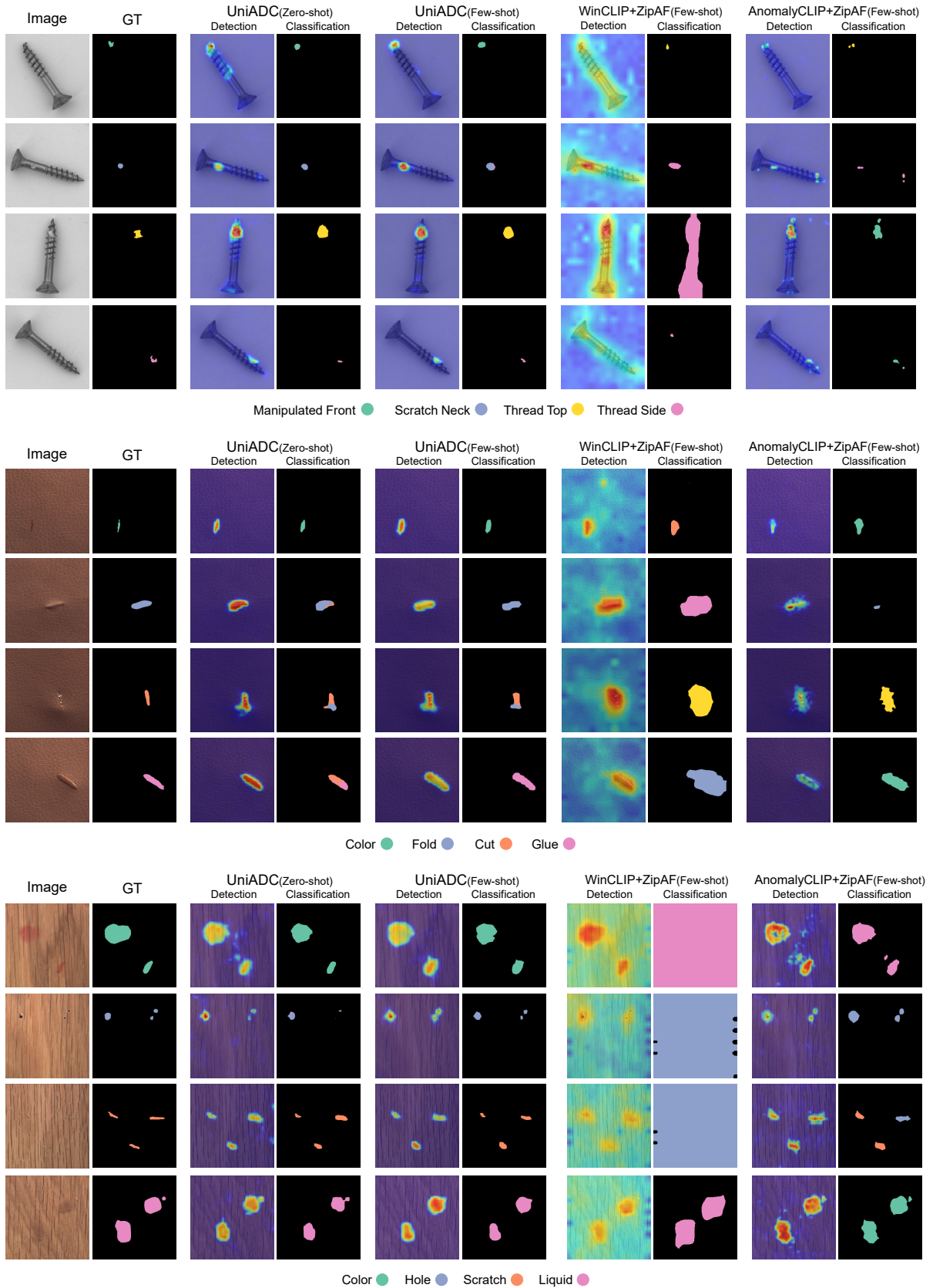


Fig. S2. Qualitative comparison of UniADC and other methods on the *Screw*, *Leather*, and *Wood* classes of the MVTec-FS dataset.

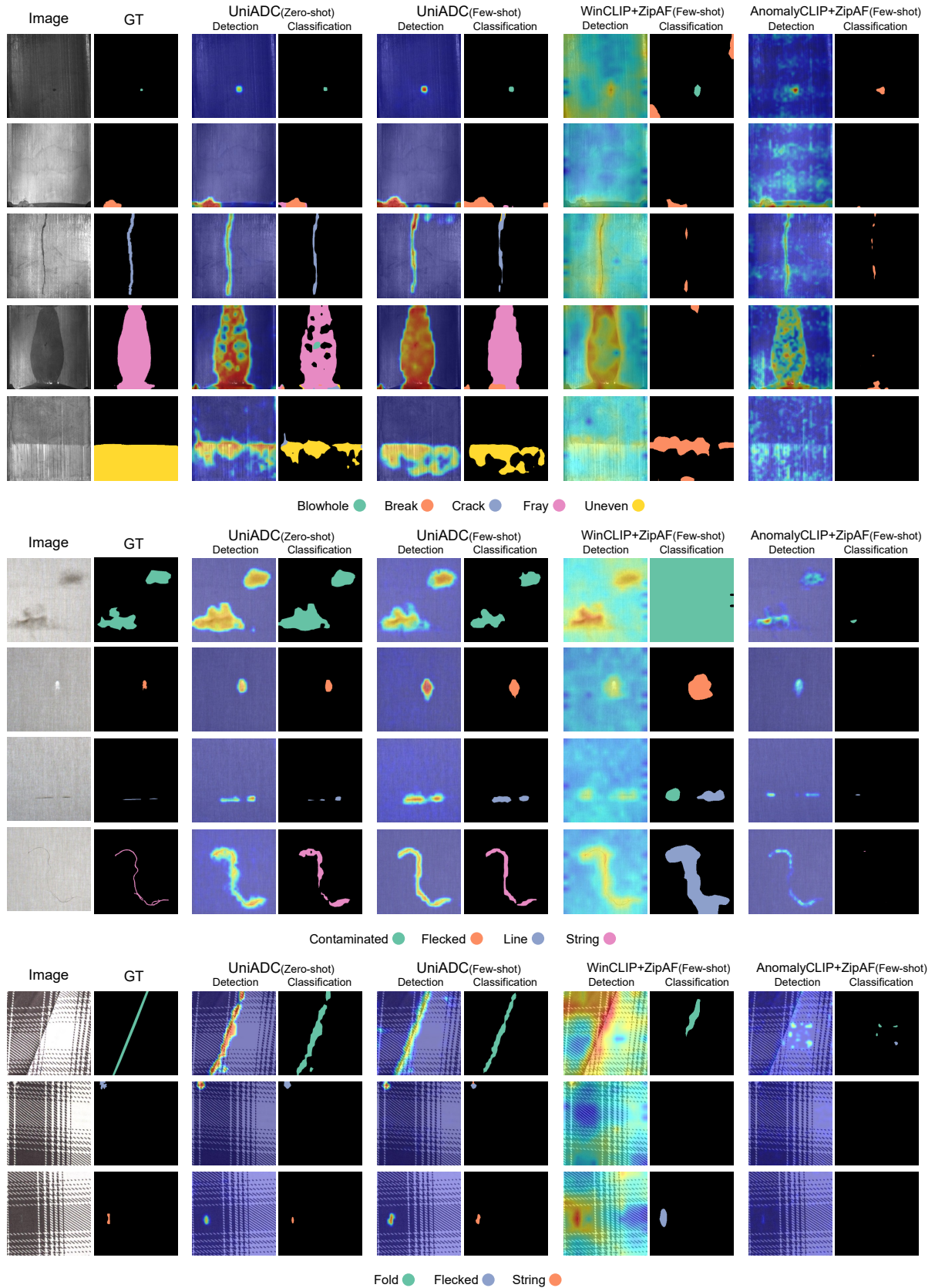


Fig. S3. Qualitative comparison of UniADC and other methods on the MTD and WFDD datasets.

TABLE S2

ANOMALY DETECTION AND CLASSIFICATION RESULTS OF **UNIADC (CLIP)** ON THE MVTEC-FS DATASET UNDER THE ZERO-SHOT ($K_n = 1$) SETTING.

	I-AUC	P-AUC	PRO	Acc	mIoU
Bottle	99.52	93.85	85.24	72.55	42.41
Cable	93.67	94.53	84.56	62.64	33.59
Capsule	90.98	97.12	92.80	43.42	24.16
Carpet	99.57	99.09	97.74	70.00	30.37
Grid	99.12	98.73	94.31	62.50	24.53
Hazelnut	99.93	98.42	95.85	75.67	29.92
Leather	100.0	99.85	98.86	77.63	39.34
Metal Nut	99.60	96.69	78.57	79.10	40.59
Pill	98.30	98.40	96.27	56.98	28.41
Screw	77.12	97.68	90.90	35.35	17.92
Tile	99.63	99.17	94.58	82.43	39.87
Toothbrush	95.00	97.05	69.96	92.59	62.76
Transistor	80.33	78.81	70.79	60.00	21.26
Wood	97.37	97.92	88.78	73.81	40.89
Zipper	95.37	97.63	92.08	46.34	17.52
AVG	95.03	96.33	88.75	66.07	32.90

TABLE S4

ANOMALY DETECTION AND CLASSIFICATION RESULTS OF **UNIADC (CLIP)** ON THE MVTEC-FS DATASET UNDER THE ZERO-SHOT ($K_n = 4$) SETTING.

	I-AUC	P-AUC	PRO	Acc	mIoU
Bottle	99.20	94.69	87.26	74.51	40.20
Cable	91.99	93.31	82.95	74.49	30.52
Capsule	96.23	97.55	94.14	63.16	28.08
Carpet	100.0	98.82	97.59	72.86	30.27
Grid	98.41	99.04	95.48	68.75	23.19
Hazelnut	99.85	98.79	95.48	81.08	39.17
Leather	99.15	99.65	99.05	76.32	39.82
Metal Nut	97.79	96.22	90.50	82.09	40.20
Pill	98.64	98.93	95.62	63.95	26.92
Screw	86.42	98.57	91.65	49.49	20.35
Tile	100.0	98.60	95.79	85.14	45.41
Toothbrush	97.78	95.18	75.49	92.59	62.41
Transistor	83.50	80.84	78.72	75.00	22.92
Wood	98.50	98.88	95.30	88.10	57.81
Zipper	95.26	97.93	92.59	52.44	19.76
AVG	96.18	96.47	91.17	73.33	35.14

TABLE S3

ANOMALY DETECTION AND CLASSIFICATION RESULTS OF **UNIADC (CLIP)** ON THE MVTEC-FS DATASET UNDER THE ZERO-SHOT ($K_n = 2$) SETTING.

	I-AUC	P-AUC	PRO	Acc	mIoU
Bottle	98.06	96.54	84.09	76.47	39.18
Cable	93.06	94.98	86.98	66.33	27.81
Capsule	89.01	94.83	90.08	61.84	26.84
Carpet	100.0	98.74	96.86	71.43	29.19
Grid	99.82	98.71	95.49	70.83	30.34
Hazelnut	99.56	99.18	94.88	85.14	44.63
Leather	100.0	99.87	97.17	75.00	35.64
Metal Nut	99.70	97.55	84.20	83.58	41.15
Pill	96.83	98.25	97.20	65.12	26.20
Screw	80.91	97.48	88.24	45.45	20.81
Tile	100.0	99.16	94.53	81.08	48.93
Toothbrush	95.56	98.16	67.10	85.19	63.61
Transistor	79.75	77.45	60.85	75.00	22.31
Wood	98.12	98.84	95.82	80.95	50.89
Zipper	98.65	98.23	94.36	51.22	19.24
AVG	95.27	96.53	88.52	71.64	35.12

TABLE S5

ANOMALY DETECTION AND CLASSIFICATION RESULTS OF **UNIADC (CLIP)** ON THE MVTEC-FS DATASET UNDER THE FEW-SHOT ($K_n = 1, K_a = 1$) SETTING.

	I-AUC	P-AUC	PRO	Acc	mIoU
Bottle	99.03	99.53	90.68	84.31	61.97
Cable	98.89	96.78	90.21	93.88	52.38
Capsule	97.70	98.24	94.09	71.05	32.34
Carpet	100.0	99.66	91.38	90.00	48.08
Grid	99.82	99.46	97.57	85.42	36.86
Hazelnut	100.0	98.50	88.62	100.0	55.76
Leather	100.0	99.85	95.80	88.16	53.67
Metal Nut	100.0	99.75	90.97	88.06	65.96
Pill	95.76	99.62	84.66	65.12	38.28
Screw	83.77	97.79	87.61	46.46	23.47
Tile	100.0	99.42	93.79	100.0	77.38
Toothbrush	95.00	97.10	71.59	92.59	59.24
Transistor	96.50	93.75	74.14	87.50	24.65
Wood	99.62	98.99	96.54	92.86	51.61
Zipper	99.30	99.54	98.14	85.37	47.66
AVG	97.69	98.53	89.72	84.72	48.62

TABLE S6

ANOMALY DETECTION AND CLASSIFICATION RESULTS OF UNIADC (CLIP) ON THE MVTEC-FS DATASET UNDER THE FEW-SHOT ($K_n = 2, K_a = 1$) SETTING.

	I-AUC	P-AUC	PRO	Acc	mIoU
Bottle	99.35	99.51	84.85	84.31	63.35
Cable	98.08	97.06	86.59	94.90	51.09
Capsule	98.11	98.54	95.52	65.79	35.10
Carpet	100.0	99.50	98.93	87.14	46.97
Grid	100.0	99.52	94.52	85.42	34.83
Hazelnut	100.0	98.16	87.54	98.65	57.38
Leather	100.0	99.85	97.10	88.16	49.87
Metal Nut	100.0	99.67	87.34	89.55	63.53
Pill	97.45	99.46	91.53	62.79	38.66
Screw	87.89	98.40	86.62	60.61	31.29
Tile	100.0	99.45	93.00	100.0	78.11
Toothbrush	98.33	96.91	85.50	92.59	64.82
Transistor	96.50	94.70	83.74	86.25	27.10
Wood	99.81	99.18	95.58	92.86	49.89
Zipper	99.73	99.54	91.30	89.02	41.97
AVG	98.35	98.63	90.64	85.20	48.93

TABLE S8

ANOMALY DETECTION AND CLASSIFICATION RESULTS OF UNIADC (CLIP) ON THE MVTEC-FS DATASET UNDER THE FEW-SHOT ($K_n = 4, K_a = 1$) SETTING.

	I-AUC	P-AUC	PRO	Acc	mIoU
Bottle	100.0	99.55	93.76	82.35	65.97
Cable	99.04	97.00	89.19	94.90	53.99
Capsule	98.85	98.23	93.57	68.42	33.75
Carpet	100.0	99.67	98.75	88.57	46.52
Grid	99.29	99.49	97.22	87.50	40.92
Hazelnut	100.0	98.27	95.95	97.30	55.50
Leather	100.0	99.85	95.94	86.84	54.37
Metal Nut	100.0	99.72	90.39	88.06	64.02
Pill	98.08	99.62	89.39	70.93	41.00
Screw	92.60	98.89	82.67	55.56	26.84
Tile	100.0	99.50	92.37	100.0	76.21
Toothbrush	96.67	97.76	78.30	92.59	65.16
Transistor	94.50	92.34	82.60	87.50	28.71
Wood	100.0	98.97	96.22	95.24	53.34
Zipper	99.52	99.46	95.03	87.80	43.81
AVG	98.57	98.55	91.42	85.57	50.01

TABLE S7

ANOMALY DETECTION AND CLASSIFICATION RESULTS OF UNIADC (CLIP) ON THE MVTEC-FS DATASET UNDER THE FEW-SHOT ($K_n = 2, K_a = 2$) SETTING.

	I-AUC	P-AUC	PRO	Acc	mIoU
Bottle	99.03	99.49	91.75	86.27	60.96
Cable	98.39	96.76	93.63	93.88	51.90
Capsule	97.29	98.83	95.44	78.95	36.03
Carpet	100.0	99.50	95.08	92.86	49.76
Grid	99.82	99.39	97.45	87.50	38.92
Hazelnut	100.0	99.71	95.57	100.0	75.10
Leather	100.0	99.84	98.46	93.42	58.77
Metal Nut	100.0	99.75	94.96	88.06	65.27
Pill	99.04	99.81	90.94	77.91	49.99
Screw	95.04	99.13	95.06	72.73	36.34
Tile	100.0	99.41	94.54	100.0	79.37
Toothbrush	96.11	97.39	78.95	92.59	65.9
Transistor	97.50	95.51	85.46	92.50	36.52
Wood	99.62	99.29	97.20	97.62	63.92
Zipper	99.35	99.42	95.10	93.90	55.24
AVG	98.75	98.88	93.31	89.88	54.93

TABLE S9

ANOMALY DETECTION AND CLASSIFICATION RESULTS OF UNIADC (CLIP) ON THE MVTEC-FS DATASET WITH FULL-SHOT NORMAL SAMPLES AND $K_a = 1$.

	I-AUC	P-AUC	PRO	Acc	mIoU
Bottle	100.0	99.68	92.40	82.35	65.17
Cable	99.35	96.77	94.87	94.90	55.04
Capsule	99.51	99.00	97.08	71.05	34.34
Carpet	100.0	99.34	95.58	88.57	47.77
Grid	99.65	99.39	96.92	89.58	42.56
Hazelnut	100.0	98.02	92.78	98.65	57.54
Leather	100.0	99.83	97.24	88.16	52.82
Metal Nut	100.0	99.74	94.11	94.03	66.48
Pill	99.04	99.68	92.54	72.09	45.28
Screw	91.34	98.92	90.67	62.63	30.26
Tile	100.0	99.44	96.61	100.0	76.79
Toothbrush	96.11	98.81	83.80	92.59	66.97
Transistor	98.25	94.12	87.52	90.00	28.23
Wood	100.0	98.65	96.34	95.24	58.06
Zipper	99.46	99.54	98.00	85.37	46.49
AVG	98.85	98.73	93.76	87.01	51.59

TABLE S10

ANOMALY DETECTION AND CLASSIFICATION RESULTS OF UNIAADC (dino) ON THE MVTEC-FS DATASET UNDER THE ZERO-SHOT ($K_n = 1$) SETTING.

	I-AUC	P-AUC	PRO	Acc	mIoU
Bottle	99.03	93.73	80.66	80.39	47.82
Cable	94.29	94.46	88.32	55.10	22.53
Capsule	94.26	98.02	93.16	59.21	26.57
Carpet	100.0	99.29	98.43	85.71	39.34
Grid	100.0	99.61	98.45	62.50	25.09
Hazelnut	99.19	98.24	80.86	75.68	38.12
Leather	100.0	99.80	96.53	80.26	39.12
Metal Nut	94.65	97.16	96.34	55.22	37.30
Pill	96.83	92.32	95.57	50.00	20.50
Screw	81.96	97.51	87.82	31.31	20.34
Tile	99.63	97.83	90.58	78.38	35.43
Toothbrush	95.00	98.87	64.09	92.59	70.73
Transistor	92.75	77.29	72.72	81.25	24.50
Wood	98.31	98.38	97.27	85.71	60.13
Zipper	99.68	99.09	96.53	51.22	18.35
AVG	96.37	96.11	89.16	68.30	35.06

TABLE S12

ANOMALY DETECTION AND CLASSIFICATION RESULTS OF UNIAADC (dino) ON THE MVTEC-FS DATASET UNDER THE ZERO-SHOT ($K_n = 4$) SETTING.

	I-AUC	P-AUC	PRO	Acc	mIoU
Bottle	99.35	96.82	94.11	82.35	56.14
Cable	92.07	95.40	90.47	71.43	29.28
Capsule	97.95	97.00	93.41	63.16	31.50
Carpet	100.0	99.63	95.21	72.86	30.93
Grid	100.0	99.60	97.57	66.67	28.54
Hazelnut	99.56	98.62	95.24	85.14	36.31
Leather	100.0	99.78	99.63	90.78	49.25
Metal Nut	99.90	98.36	94.95	82.09	37.84
Pill	97.79	96.11	97.90	56.98	21.66
Screw	88.44	97.86	91.35	55.56	20.66
Tile	98.45	98.07	95.64	86.49	43.62
Toothbrush	100.0	96.90	73.31	100.0	63.42
Transistor	95.00	88.84	79.31	86.25	26.01
Wood	98.12	99.16	97.04	88.10	59.55
Zipper	98.06	98.27	95.05	57.32	23.80
AVG	97.65	97.36	92.68	76.35	37.23

TABLE S11

ANOMALY DETECTION AND CLASSIFICATION RESULTS OF UNIAADC (dino) ON THE MVTEC-FS DATASET UNDER THE ZERO-SHOT ($K_n = 2$) SETTING.

	I-AUC	P-AUC	PRO	Acc	mIoU
Bottle	98.39	97.81	93.78	82.35	54.97
Cable	92.53	96.26	87.31	65.31	23.65
Capsule	98.52	98.78	97.59	61.84	32.78
Carpet	99.66	98.71	97.98	81.43	34.54
Grid	100.0	99.61	96.57	72.92	31.05
Hazelnut	99.63	97.53	91.29	85.14	38.84
Leather	99.93	99.52	98.39	82.89	41.56
Metal Nut	99.39	98.05	97.08	79.10	42.24
Pill	95.98	88.81	96.12	58.14	23.38
Screw	88.98	98.25	91.98	55.56	26.93
Tile	99.48	98.66	94.62	78.38	34.05
Toothbrush	99.44	97.19	79.21	96.30	68.10
Transistor	92.92	89.11	69.53	77.50	21.62
Wood	93.61	98.95	96.26	88.10	56.52
Zipper	97.95	98.36	94.50	56.10	19.73
AVG	97.09	97.04	92.15	74.74	36.66

TABLE S13

ANOMALY DETECTION AND CLASSIFICATION RESULTS OF UNIAADC (dino) ON THE MVTEC-FS DATASET UNDER THE FEW-SHOT ($K_n = 1, K_a = 1$) SETTING.

	I-AUC	P-AUC	PRO	Acc	mIoU
Bottle	99.52	99.71	88.05	82.35	61.95
Cable	96.74	96.77	90.09	92.86	54.27
Capsule	99.51	99.26	96.03	76.32	36.23
Carpet	100.0	99.81	98.04	81.43	45.19
Grid	100.0	99.51	96.77	91.67	41.38
Hazelnut	100.0	98.36	93.94	100.0	54.67
Leather	100.0	99.84	96.65	93.42	50.08
Metal Nut	99.90	99.74	94.22	88.06	65.78
Pill	95.48	99.67	79.47	66.28	40.39
Screw	85.58	99.17	88.31	54.55	30.12
Tile	100.0	99.44	96.31	98.65	74.52
Toothbrush	100.0	97.73	81.59	100.0	67.76
Transistor	100.0	96.68	92.18	91.25	30.78
Wood	99.62	99.03	94.94	92.86	57.39
Zipper	99.95	99.72	97.24	91.46	58.72
AVG	98.42	98.96	92.26	86.74	51.28

TABLE S14

ANOMALY DETECTION AND CLASSIFICATION RESULTS OF UNIA DC (dino) ON THE MVTEC-FS DATASET UNDER THE FEW-SHOT ($K_n = 2, K_a = 1$) SETTING.

	I-AUC	P-AUC	PRO	Acc	mIoU
Bottle	100.0	99.69	90.82	82.35	61.38
Cable	97.28	97.22	85.47	93.88	56.36
Capsule	98.28	99.18	95.61	75.00	38.77
Carpet	100.0	99.41	98.48	81.43	43.57
Grid	100.0	99.58	96.91	91.67	37.38
Hazelnut	100.0	99.12	95.51	98.65	54.04
Leather	100.0	99.83	96.21	93.42	50.59
Metal Nut	100.0	99.77	93.91	89.55	65.82
Pill	97.17	99.60	87.16	68.60	40.80
Screw	88.10	98.98	86.88	62.63	31.49
Tile	100.0	99.31	96.79	98.65	75.22
Toothbrush	98.33	97.13	87.94	92.59	68.74
Transistor	99.92	96.25	86.5	91.25	29.50
Wood	99.25	98.73	94.72	92.86	57.74
Zipper	100.0	99.72	94.34	90.24	60.95
AVG	98.56	98.90	92.48	86.85	51.49

TABLE S16

ANOMALY DETECTION AND CLASSIFICATION RESULTS OF UNIA DC (dino) ON THE MVTEC-FS DATASET UNDER THE FEW-SHOT ($K_n = 4, K_a = 1$) SETTING.

	I-AUC	P-AUC	PRO	Acc	mIoU
Bottle	99.68	99.65	92.64	82.35	64.09
Cable	97.82	96.17	86.18	92.86	56.49
Capsule	99.10	99.24	92.04	76.32	39.26
Carpet	100.0	99.23	98.07	84.29	45.52
Grid	100.0	99.59	96.08	91.67	38.76
Hazelnut	100.0	99.03	98.33	95.95	55.39
Leather	100.0	99.83	96.81	89.47	54.12
Metal Nut	100.0	99.79	92.50	86.57	65.63
Pill	97.51	99.66	92.65	69.77	43.59
Screw	87.55	98.97	89.40	57.58	27.68
Tile	100.0	98.55	97.52	100.0	74.99
Toothbrush	100.0	98.26	86.35	100.0	69.02
Transistor	99.83	97.00	89.72	91.25	33.87
Wood	99.06	98.97	93.59	92.86	58.14
Zipper	100.0	99.74	98.44	91.46	59.02
AVG	98.70	98.91	93.35	86.83	52.37

TABLE S15

ANOMALY DETECTION AND CLASSIFICATION RESULTS OF UNIA DC (dino) ON THE MVTEC-FS DATASET UNDER THE FEW-SHOT ($K_n = 2, K_a = 2$) SETTING.

	I-AUC	P-AUC	PRO	Acc	mIoU
Bottle	100.0	99.67	94.18	84.31	55.23
Cable	98.05	97.93	89.26	87.76	45.81
Capsule	98.93	99.10	92.47	77.63	40.49
Carpet	99.66	99.70	98.77	88.57	50.76
Grid	100.0	99.63	96.01	87.50	41.06
Hazelnut	100.0	99.78	95.58	97.30	70.42
Leather	100.0	99.82	96.77	93.42	52.75
Metal Nut	100.0	99.76	95.22	88.06	66.13
Pill	99.21	99.81	93.64	73.26	51.18
Screw	89.96	99.13	95.36	72.73	36.34
Tile	100.0	99.30	98.23	100.0	77.04
Toothbrush	100.0	97.30	83.60	96.30	66.82
Transistor	99.92	96.76	85.19	91.25	38.44
Wood	100.0	99.12	94.82	97.62	60.69
Zipper	100.0	99.67	94.12	95.12	59.93
AVG	99.05	99.10	93.55	88.72	54.21

TABLE S17

ANOMALY DETECTION AND CLASSIFICATION RESULTS OF UNIA DC (dino) ON THE MVTEC-FS DATASET WITH FULL-SHOT NORMAL SAMPLES AND $K_a = 1$.

	I-AUC	P-AUC	PRO	Acc	mIoU
Bottle	100.0	99.71	94.61	78.43	58.28
Cable	97.66	96.48	90.91	94.90	56.25
Capsule	99.26	99.33	95.31	75.00	42.60
Carpet	99.92	99.23	96.55	82.86	42.77
Grid	100.0	99.59	96.71	85.42	42.41
Hazelnut	100.0	98.65	92.32	97.30	55.91
Leather	100.0	99.85	96.04	92.11	52.04
Metal Nut	100.0	99.78	94.00	89.55	66.52
Pill	99.32	99.62	89.46	72.09	44.18
Screw	95.21	99.00	90.42	74.75	31.86
Tile	100.0	99.34	97.99	100.0	75.35
Toothbrush	100.0	97.10	94.60	100.0	67.21
Transistor	100.0	97.87	89.15	90.00	34.11
Wood	99.81	98.99	97.04	95.24	53.83
Zipper	100.0	99.68	95.79	90.24	55.70
AVG	99.41	98.95	94.06	87.86	51.93

TABLE S18
ANOMALY DETECTION AND CLASSIFICATION RESULTS OF
UNIADC (CLIP) ON THE WFDD DATASET UNDER THE ZERO-SHOT
($K_n = 1$) SETTING.

	I-AUC	P-AUC	PRO	Acc	mIoU
Grey Cloth	99.89	99.08	85.75	81.25	38.05
Grid Cloth	94.51	98.10	78.98	90.00	44.08
Pink Flower	95.18	99.90	90.85	85.71	55.14
Yellow Cloth	98.46	98.92	92.54	89.82	44.93
AVG	97.01	99.00	87.03	86.70	45.55

TABLE S22
ANOMALY DETECTION AND CLASSIFICATION RESULTS OF
UNIADC (CLIP) ON THE WFDD DATASET UNDER THE FEW-SHOT
($K_n = 2, K_a = 1$) SETTING.

	I-AUC	P-AUC	PRO	Acc	mIoU
Grey Cloth	99.67	98.80	95.53	92.19	42.92
Grid Cloth	97.41	98.62	94.95	89.00	41.42
Pink Flower	98.96	99.98	93.74	96.43	68.46
Yellow Cloth	99.85	99.23	94.35	97.01	46.04
AVG	98.97	99.16	94.64	93.66	49.71

TABLE S19
ANOMALY DETECTION AND CLASSIFICATION RESULTS OF
UNIADC (CLIP) ON THE WFDD DATASET UNDER THE ZERO-SHOT
($K_n = 2$) SETTING.

	I-AUC	P-AUC	PRO	Acc	mIoU
Grey Cloth	99.11	98.67	84.78	92.19	42.70
Grid Cloth	95.43	98.56	79.80	86.00	41.23
Pink Flower	97.27	99.90	91.49	89.29	62.02
Yellow Cloth	98.39	98.79	92.47	90.42	46.64
AVG	97.55	98.98	87.14	89.48	48.15

TABLE S23
ANOMALY DETECTION AND CLASSIFICATION RESULTS OF
UNIADC (CLIP) ON THE WFDD DATASET UNDER THE FEW-SHOT
($K_n = 2, K_a = 2$) SETTING.

	I-AUC	P-AUC	PRO	Acc	mIoU
Grey Cloth	99.11	98.89	95.70	93.75	42.85
Grid Cloth	98.75	99.11	93.07	90.00	43.64
Pink Flower	98.70	99.97	95.06	96.43	67.73
Yellow Cloth	100.0	99.40	95.55	99.40	50.02
AVG	99.14	99.34	94.85	94.90	51.06

TABLE S20
ANOMALY DETECTION AND CLASSIFICATION RESULTS OF
UNIADC (CLIP) ON THE WFDD DATASET UNDER THE ZERO-SHOT
($K_n = 4$) SETTING.

	I-AUC	P-AUC	PRO	Acc	mIoU
Grey Cloth	99.89	98.95	90.16	95.32	42.74
Grid Cloth	94.42	98.51	75.61	83.00	41.52
Pink Flower	98.96	99.67	96.86	92.86	62.84
Yellow Cloth	99.34	99.22	90.51	92.22	45.85
AVG	98.15	99.09	88.29	90.85	48.24

TABLE S24
ANOMALY DETECTION AND CLASSIFICATION RESULTS OF
UNIADC (CLIP) ON THE WFDD DATASET UNDER THE FEW-SHOT
($K_n = 4, K_a = 1$) SETTING.

	I-AUC	P-AUC	PRO	Acc	mIoU
Grey Cloth	99.78	98.67	92.77	92.19	42.24
Grid Cloth	98.06	98.89	94.81	90.00	42.79
Pink Flower	99.61	99.97	95.55	96.43	67.80
Yellow Cloth	99.94	99.24	94.80	97.01	46.92
AVG	99.35	99.19	94.48	93.91	49.94

TABLE S21
ANOMALY DETECTION AND CLASSIFICATION RESULTS OF
UNIADC (CLIP) ON THE WFDD DATASET UNDER THE FEW-SHOT
($K_n = 1, K_a = 1$) SETTING.

	I-AUC	P-AUC	PRO	Acc	mIoU
Grey Cloth	99.78	98.08	88.76	92.19	39.84
Grid Cloth	95.76	98.68	92.87	89.00	40.55
Pink Flower	98.70	99.97	95.56	96.43	68.70
Yellow Cloth	99.77	98.60	94.63	96.41	45.93
AVG	98.50	98.83	92.96	93.51	48.76

TABLE S25
ANOMALY DETECTION AND CLASSIFICATION RESULTS OF
UNIADC (CLIP) ON THE WFDD DATASET WITH FULL-SHOT NORMAL
SAMPLES AND $K_a = 1$.

	I-AUC	P-AUC	PRO	Acc	mIoU
Grey Cloth	99.67	98.91	94.10	92.19	42.21
Grid Cloth	98.30	98.55	95.79	90.00	44.99
Pink Flower	99.87	99.98	95.34	98.21	67.60
Yellow Cloth	99.94	99.22	96.88	98.20	47.46
AVG	99.45	99.17	95.53	94.65	50.57

TABLE S26
ANOMALY DETECTION AND CLASSIFICATION RESULTS OF
UNIADC (dino) ON THE WFDD DATASET UNDER THE ZERO-SHOT
($K_n = 1$) SETTING.

	I-AUC	P-AUC	PRO	Acc	mIoU
Grey Cloth	99.11	99.11	85.80	71.88	36.15
Grid Cloth	95.76	99.29	92.48	92.00	52.53
Pink Flower	97.66	99.94	93.57	94.64	66.77
Yellow Cloth	99.77	99.49	96.65	97.01	53.24
AVG	98.08	99.46	92.13	88.88	52.17

TABLE S30
ANOMALY DETECTION AND CLASSIFICATION RESULTS OF
UNIADC (dino) ON THE WFDD DATASET UNDER THE FEW-SHOT
($K_n = 2, K_a = 1$) SETTING.

	I-AUC	P-AUC	PRO	Acc	mIoU
Grey Cloth	99.78	99.03	90.87	96.88	42.32
Grid Cloth	99.72	99.45	97.17	95.00	49.43
Pink Flower	100.0	99.97	92.74	98.21	68.35
Yellow Cloth	99.97	99.46	95.68	98.80	47.02
AVG	99.87	99.48	94.12	97.22	51.78

TABLE S27
ANOMALY DETECTION AND CLASSIFICATION RESULTS OF
UNIADC (dino) ON THE WFDD DATASET UNDER THE ZERO-SHOT
($K_n = 2$) SETTING.

	I-AUC	P-AUC	PRO	Acc	mIoU
Grey Cloth	99.89	99.22	84.57	73.44	38.96
Grid Cloth	94.91	99.15	93.18	90.00	51.90
Pink Flower	98.18	99.91	94.48	96.43	69.34
Yellow Cloth	99.84	99.57	97.15	97.01	53.33
AVG	98.21	99.46	92.35	89.22	53.38

TABLE S31
ANOMALY DETECTION AND CLASSIFICATION RESULTS OF
UNIADC (dino) ON THE WFDD DATASET UNDER THE FEW-SHOT
($K_n = 2, K_a = 2$) SETTING.

	I-AUC	P-AUC	PRO	Acc	mIoU
Grey Cloth	99.89	99.00	94.57	98.44	46.38
Grid Cloth	99.84	99.44	96.82	95.00	46.76
Pink Flower	100.0	99.98	91.60	100.0	67.73
Yellow Cloth	100.0	99.54	93.77	97.60	46.78
AVG	99.93	99.49	94.19	97.76	51.91

TABLE S28
ANOMALY DETECTION AND CLASSIFICATION RESULTS OF
UNIADC (dino) ON THE WFDD DATASET UNDER THE ZERO-SHOT
($K_n = 4$) SETTING.

	I-AUC	P-AUC	PRO	Acc	mIoU
Grey Cloth	100.0	99.33	90.00	73.44	40.04
Grid Cloth	94.38	98.72	95.09	92.00	51.85
Pink Flower	100.0	99.96	95.67	100.0	74.90
Yellow Cloth	100.0	99.56	98.26	98.80	54.98
AVG	98.60	99.39	94.76	91.06	55.44

TABLE S32
ANOMALY DETECTION AND CLASSIFICATION RESULTS OF
UNIADC (dino) ON THE WFDD DATASET UNDER THE FEW-SHOT
($K_n = 4, K_a = 1$) SETTING.

	I-AUC	P-AUC	PRO	Acc	mIoU
Grey Cloth	99.78	98.91	94.05	96.88	43.22
Grid Cloth	99.68	99.53	94.24	95.00	46.77
Pink Flower	100.0	99.97	94.17	100.0	69.40
Yellow Cloth	100.0	99.38	95.88	98.80	47.79
AVG	99.87	99.45	94.59	97.67	51.80

TABLE S29
ANOMALY DETECTION AND CLASSIFICATION RESULTS OF
UNIADC (dino) ON THE WFDD DATASET UNDER THE FEW-SHOT
($K_n = 1, K_a = 1$) SETTING.

	I-AUC	P-AUC	PRO	Acc	mIoU
Grey Cloth	99.67	98.74	89.51	92.19	42.52
Grid Cloth	99.72	99.41	96.11	94.00	45.38
Pink Flower	100.0	99.98	95.19	100.0	68.18
Yellow Cloth	99.99	99.35	95.48	98.20	46.03
AVG	99.85	99.37	94.07	96.10	50.53

TABLE S33
ANOMALY DETECTION AND CLASSIFICATION RESULTS OF
UNIADC (dino) ON THE WFDD DATASET WITH FULL-SHOT NORMAL
SAMPLES AND $K_a = 1$.

	I-AUC	P-AUC	PRO	Acc	mIoU
Grey Cloth	100.0	98.82	95.95	97.14	40.78
Grid Cloth	99.96	99.51	94.90	95.00	48.75
Pink Flower	100.0	99.97	95.92	100.0	70.59
Yellow Cloth	99.97	99.44	94.58	98.80	49.85
AVG	99.98	99.44	95.34	97.74	52.49